12-2015

The Mass-Pitch Angle Relation for Three High Redshift Active Galaxies Selected from the GOODS Field

John Adam Hughes
University of Arkansas, Fayetteville

The Mass-Pitch Angle Relation for Three High Redshift Active Galaxies Selected from the GOODS Field

A thesis submitted in partial fulfillment
of the requirements for the degree of
Master of Science in Space and Planetary Sciences

by

John Hughes
Henderson State University
Bachelor of Science in Physics, 2007

December 2015
University of Arkansas

This thesis is approved for recommendation to the Graduate Council

---

Dr. Julia Kennefick
Thesis Director:

Dr. Paul M. Thibado
Committee member

Dr. Claud H. Sandberg Lacy
Committee member

Dr. Larry Roe
Committee member

Abstract

As we continue to investigate and ponder the heavens, we have come to realize the presence of highly energetic gravitational wells at the center of all galaxies. These supermassive black holes at a galaxies nucleus formed in the company of the other features making up the galaxy, particularly spiral arms. With nearby galaxies showing a relationship between the spiral arm pitch angle and that central mass, here we push that relationship out to distances of redshift one. With three galaxies at this distance we find that they also hold to the same relationship of tighter spiral arms corresponding to more massive central black holes. We find that these three galaxies near a redshift of one also fit the equation $\log \frac{M}{M_\odot} = (8.21 \pm 0.16) - (0.062 \pm 0.009)P$ given by Berrier et al. (2013) for nearby spiral galaxies. Further investigation of higher signal to noise spectroscopic observations will increase this confidence and demonstrate the robustness of the $M - P$ relationship at greater distances.

Dedication

Jack L. Turner Sr., who nurtured curiosity throughout my life.

Acknowledgements

This research was carried out at the Arkansas Center for Space and Planetary Sciences with Julia Kennefick, Department of Physics, University of Arkansas Fayetteville, with the Arkansas Galaxy Evolution Survey (AGES) research team.

Funding for this research comes from the NASA Space Grant EpSCoR Grant (NNX08AWO3A) for the Arkansas Galaxy Evolution Survey (AGES) and the University of Arkansas.

This research has made use of the NASA/IPAC Extragalactic Database (NED) which is operated by the Jet Propulsion Laboratory, California Institute of Technology, under contract with the National Aeronautics and Space Administration.

Table of Contents

List of Figures

List of Tables

1 Introduction

Motivation for this study comes down through many generations, from the time man started to wonder where he came from and where the planet we call home came from. To this end, we have studied archeological sites which reveal to us objects left behind by our forefathers over millennia. Farther back, we look at the geological processes which result from millions of years of sedimentation and erosion of the Earth's surface and crust as it evolves on this planet, which is unique in that it is unlike any other planet we have seen in the heavens. Farther out from our star we begin to study our history in a totally different way. Because our universe is so vast, when we look at our nearest neighbor star, Proxima Centauri, we are seeing it as it was over four years ago.

At this scale the speed of light is low enough that we are no longer making inferences about the past from objects that have aged relatively little, rather we are actually seeing the past. Our nearest neighbor galaxy, M31 in Andromeda, is similar to our own, but we see it as it was two million years ago. The spiral galaxies we will study in this paper provide glimpses of galaxies as they were over five billion years ago.

In 1924 Edwin Hubble presented evidence of other galaxies outside of our Milky Way galaxy (Hubble, 1929). In the Andromeda galaxy, he discovered a Cepheid variable star which allowed him to determine its distance. This ended the dispute of whether or not spiral nebulae were outside of our galaxy and ushered in the study of distant galaxies. Although types of galaxies include ellipticals and irregulars, we are going to focus entirely on spiral galaxies. These large collections of gas, dust, stars and planets are held together by gravity, with the density of ordinary matter highest in the central region or nucleus.

This central region or nucleus of the galaxy is generally accepted to have at its center, a supermassive black hole (SMBH). What we are seeing now is the black hole mass as it was before, because the travel time for light to reach us is many billion years. The state of a galaxy we see today is that of a former time. We are living on the Earth now and seeing the universe as it was. What is the universe now? It only took ten minutes to make tea (1.90×10^{-11} Myrs). By studying the distant galaxies, with look back times of billions of years, we are studying a time before Earth's formation.

Galaxies known as quasi-stellar radio source objects, first thought to be nearby stars,

are distant galaxies with more energy radiating from the nuclear region than the rest of the galaxy. The discovery of these objects lead astronomers and physicists to think about enormous amounts of energy densely packed into a small volume (Schmidt, 1963; Hazard, 1964; Burbidge et al., 1963; Greenstein & Schmidt, 1964). Black holes were theorized to be the source of this energy, but in this case, a new class of black holes a million to a billion times the mass of our Sun, a supermassive black hole. Active Galactic Nuclei (AGN) became a sub class of galaxies including the quasars and other galaxies displaying a large amount of energy emanating from the nucleus of the galaxy.

1.1 AGN

The current unified model for AGN features an obscuring torus of gas and dust around the central black hole in the galaxy's central broad line region. This torus region is composed of gas clouds which obscure the broad line region emission depending on the orientation of the AGN. The narrow line region is located outside the realm of the obscuring torus and therefore is not obscured at any orientation.

Seyfert galaxies where first described by Carl Seyfert (Seyfert, 1946). Seyfert galaxies are similar to quasars spectroscopically with the exception of the host galaxy being visible. This usually means that the quasars are at greater distances and more luminous than Seyferts.

The narrow emission lines are observed in both Seyfert 1 and 2 galaxies. Seyfert 1 galaxies display a broad line region (BLR) and a narrow line region (NLR) and therefore, in this model, the line of sight is not obscured by the torus. Seyfert 2 galaxies do not display a broad line region but do exhibit a narrow line region and therefore, in this model, the line of sight to the broad line region is obscured by the torus.

The unified model for AGN describes these active galaxies to typically be of the same fueling mechanisms, with the majority of the energy output coming from the central region but classified differently according to the orientation or point of view.

Through the unified model, we understand this to be associated with the idea that an obscuring torus of gas and dust lies outside of the broad line region. The narrow line region lies outside the radius of the torus and therefor can not be obscured by the torus, where the broad line region may be obscured, depending on the orientation.

Studying the polarity of the emission coming from the central region gave way to the

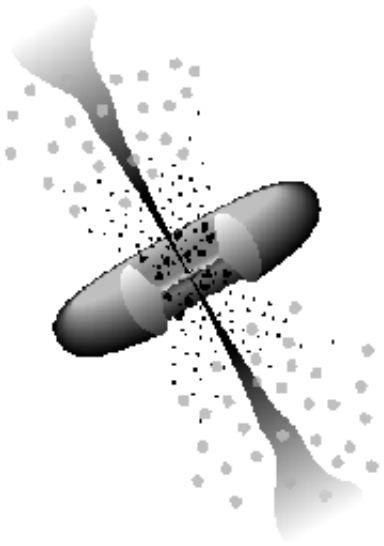

Figure 1.1: Cartoon depicting the angles at which the torus blocks the Broad Line Region from the unified theory of AGN. With the BLR represented by the larger black dots within the torus, one can see through the cut away as to how this emission would be blocked by the torus if the observer where seeing the AGN edge on with respect to the torus. The NLR on the other hand, can be seen from any viewing angle because the emission is coming from the smaller black dots. (Urry & Padovani, 1995)

interpretation of a torus obscuring the broad lines (Bianchi et al., 2012; Krolik & Begelman, 1988; Wilkes et al., 1995).

In the case of NGC 1068 we are able to see some of this reflected, therefor highly polarized, light from the broad line region. A simple medium blocking the view of the emitted light would not achieve this effect, giving a summation of the polarity would cancel each other out. The reason for the torus comes from modeling of the observed polarity and being the best explanation for the observed polarization.

The process of accretion around a supermassive black hole results from a very strong gravitational well. Gas and dust orbiting the central mass accelerate to velocities high enough to emit X-rays and gamma rays. Accretion onto a supermassive black hole is modeled to be the high luminosity energy source we see emanating from the center of some galaxies.

Experimental evidence for accretion onto a black hole comes from the observations of sub-arc-second variations in the spectral signature from this region, putting an upper limit on the size of the central mass (Peterson, 1993).

Quasi-stellar radio sources, quasars, where discovered in the 1960's and generated much debate as their redshifts were greater than previously detected for any object (Schmidt,

1963). This implied that their energy output was far greater than what was possible for stellar mass objects. Also mysterious, were the broad emission lines observed in the spectra. Over the next decades, quasars were modeled to be a type of AGN with a particular orientation, the most distant objects known, and the power source to be the accretion of gas and dust in the gravitational well of a supermassive black hole at the center of the galaxy. Moderate redshift quasars tend to be bluer than other distant galaxies and with stronger emission lines. This, bluer UV excess, is also used as a technique for finding quasar candidates in imaging surveys (Peterson, 1997).

The nuclear region absolute magnitude for a quasar is $M_B < -21.5 + 5 \log h_0$, which is the most luminous of all AGN (Peterson, 1997).

The quasar category has evolved since the early discovery of a "quasi-stellar radio source" to include non-radio sources as well. The strong radio source type of quasar that was first discovered now only constitutes $5 - 10\%$ of the quasar population (Peterson, 1997).

The term AGN applies to a broad classification of galaxies, including quasars, that exhibit a powerful emission of electromagnetic radiation across the entire spectrum from radio wave to gamma ray frequencies, originating from the central region of the galaxy and in many cases overwhelms the total emission of the entire galaxy. This characteristic of AGN allows for identification from many different observatories including X-ray observatories like the Chandra X-ray observatory orbiting the Earth. If a point source of X-ray radiation is observed from a distant source with a significant absolute magnitude, indicating enormous energy generation in a relatively small area, a supermassive black hole gravitationally accreting/energizing material is our most likely candidate.

The broad spectra of AGN are easily distinguished from the thermal blackbody spectrum of a star or even the combined spectra of many stars, such as in a galaxy (Carroll & Ostlie, 2007). Sources of X-ray continuum are radiating thermal spectra from very hot material, or non-thermal processes from very energy-rich material (Osterbrock & Ferland, 2006). The spectra of an AGN is very different from that of a star alone or a galaxy and its stars (Carroll & Ostlie, 2007). When X-rays are observed as continuum sources, they are originating from a very energy rich area such as energy rich material radiating synchrotron emission (Osterbrock & Ferland, 2006).

When identfying AGN with Chandra X-ray observatory data, we use a luminosity cutoff to separate X-ray starburst galaxies from AGN of $L_{0.5-10}$ keV $> 3 \times 10^{42}$ erg s^{-1} (Trump et al., 2011).

During the early days with the discovery of quasars and other AGN there was a need to explain the massive amounts of energy emitted from such a small area.

Soon, it was realized, through relationships formed between host galaxy properties and black hole mass, that even galaxies not exhibiting activity in the nuclei also hosted supermassive black holes. These relationships include the M_{bh} to bulge luminosity relation and the M_{bh} to velocity dispersion relation (Kormendy & Richstone, 1995; Ferrarese & Merritt, 2000; Gebhardt et al., 2000).

1.2 Mass-Pitch Angle Relation

Seigar et al. (2008) discovered the M-P (M_{bh} to spiral arm Pitch angle) relationship that shows there to be a correlation between M and P for nearby spiral galaxies. In order to fully exploit this relationship to study the evolution of galaxies, we must push the relationship to greater look-back times and confirm whether or not the relationship it true at greater distances. In order to do this we focus on previous methods for estimating central SMBH mass at greater look-back times such as reverberation mapping, mass scaling relationships, the fundamental plane of black holes, velocity dispersion, and bulge luminosity. In order to make these measurements for mass scaling relationships the galaxy must exhibit broad emission lines in its spectrum.

1.3 Mass-Pitch Angle Relation at greater Look-back Time

In this thesis we look at spiral galaxies with active galactic nuclei (AGN), at redshift near 1, in order to determine if the M-P relationship holds for galaxies earlier in their evolutionary life time, i.e. further look back time. We will describe the process for selecting these AGN with spiral structure and the method used for measuring the spiral arm pitch angle along with some of the difficulties arising at these greater distances and lower resolution. Then we will discuss the method by which we compare the black hole mass from the M-P relationship, which is a mass scaling relationship using single epoch spectra broad line measurements and continuum luminosity as proxies for velocity and radius of material orbiting the black hole respectively. Finally, the results will show the trend for the M-P relationship at $z \approx 1$.

A general consensus by astronomers and physicists today is that most galaxies harbor a supermassive black hole at their center, with masses ranging from less than a million to

more than a billion solar masses (Magorrian et al., 1998). Furthermore, galaxies with an active galactic nucleus are considered to be otherwise normal galaxies with the difference being the SMBH is actively accreting material causing a very bright central region which emits throughout the entire electromagnetic spectrum (Elvis et al., 1994). The standard model of AGN holds that the quasars, blazars, radio galaxies and all type of AGN are the same type of galaxy just being viewed at different orientations (Tadhunter, 2008).

The velocity dispersion of the material orbiting the central SMBH can be extrapolated from the broad emission lines in their spectra. Assuming the orbiting material is virialized and in a Keplarian orbit, the only other information needed to estimate the mass, contained within this radius, is the distance at which the material is orbiting.

The broad lines observed in the spectra of distant objects are broadened in part by the expansion of the universe which results in a stretching of the spectral line proportional to the amount of the redshift, z, although the broad lines seen in AGN spectra are much broader than expansion can explain. Additional broadening is caused by high velocities that can only be explained by the orbiting of material in a gravitational well proportional to a mass of 10^6 to 10^9 $M_\odot$.

1.4 Mass Determination

1.4.1 Reverberation Mapping

Reverberation mapping is a technique used to determine the distance at which material from a specific emission region is orbiting a central gravitational source (Peterson, 1993). A region we call the Broad Line Region (BLR). The technique monitors the central source to look for variations in the continuum brightness and a fluctuation in a specific spectral emission emanating from the BLR. This region is theorized to be a tours shape region of gas clouds orbiting the central gravitational well with ionized gases that can only exist in an environment of this nature. Some time after the continuum brightness increases, usually a lapse of a few days, an emission line in the monitored spectra will also increase. Think of a torus with a source at its center and this increased continuum is the matter being accreted and emitting radiation out toward the torus where, at some time later, the gases in the torus are excited. Taking this emission region time lapse and assuming the radiating energy is transferred at the speed of light, c, from the central region to the excited gas emission region, a distance from the central source can be calculated. We are confident in this theory,

because of the level of ionized gas accounts for the conditions at which they are limited to exist in and the energy needed to emit this amount of radiation. Combining these two reasons, we are also confident because of the time scale at which we are seeing these fluctuations must be confined by the limit of the speed of light, albeit over the large gathering area at which the spectrograph is detecting photons.

1.4.2 Scaling Relation

A scaling relationship is then formed between the continuum luminosity at a specific wavelength and the BLR radius (Vestergaard & Peterson, 2006; McLure & Jarvis, 2002).

We use a relationship that scales the MgII line FWHM to the orbital velocity (McLure & Jarvis, 2002; McGill et al., 2008). This can be measured from single epoch spectroscopic measurements.

1.5 Related to Host Galaxy Properties

1.5.1 Velocity Dispersion

Velocity Dispersion is measured by observing the broadening of emission lines. This line is physically widened due to the random orbital paths of stars, with the stars orbiting in the approaching direction blue shifting the emission and the stars orbiting in the recessing direction being red shifted, as the velocity dispersion defines the separation of the λ_o emission. The dispersed radial velocity of the stars creates a Gaussian distribution around the average velocity, λ_o ($km\ s^{-1}$), the rest wavelength of the observed emission line.

A measure of the orbiting stars is observed in the central region of the bulge, σ_c the velocity dispersion, which also allows for a correlation to be formed between the black hole mass and a luminosity-weighted line-of-sight velocity dispersion (Ferrarese & Merritt, 2000; Gebhardt et al., 2000).

1.5.2 Bulge Luminosity

Bulge luminosity and central black hole mass show a looser correlation than the velocity dispersion and central black hole mass (Ferrarese & Merritt, 2000). This relationship has a greater scatter at lower mass black holes. The relationship is intuitively not sound, because of the distance of the bulge from the central gravitational source, the supermassive black hole, being out of the gravitational influence of the central mass. Although some

authors theorize that the relationship is due to the idea that the bulge mass and the black hole mass grew together in the same environment (Ferrarese & Merritt, 2000).

1.5.3 Black Hole Mass

Central SMBH mass has, in the past, been correlated with bulge luminosity by Kormendy et al. (2000) and then Seigar et al. (2008) makes the relationship known for the direct correlation of black hole mass and spiral arm pitch angle.

The most stunning example and strongest evidence for the existence of supermassive black holes comes from our own milky way galaxy center, where the direct measurement of stars, stellar kinematics, orbiting a central gravitational well is observed (Ghez et al., 2005). In one case a star is observed and tracked through one complete orbit. Through the observations of these stars orbiting this massive gravitational well a mass is calculated of $(3.7 \pm 0.2) \times 10^6 \ M_{sun}$ (Ghez et al., 2005). When measuring the rotational velocity of material orbiting the black hole, stellar measurements are more reliable because their influence is primarily gravitational, whereas gas and dust, which can orbit closer to the Schwarzschild radius, may have a greater magnetic component affecting the orbital velocity (Kormendy & Richstone, 1995). Other techniques for determining the existence and mass of these central massive dark objects, comes from the observation of gas and dust orbiting in the nuclear region. Through this measurement a virial mass is calculated, which is the total mass within the virial radius of orbiting gas and dust. This method is considered accurate because the mass of the black hole is much greater than the other material within the virial radius. Reverberation mapping gathers information about the change in continuum luminosity as a function of time, by gathering spectroscopic observations over a period of months. This change is observed as being the precursor to increased intensity of emission lines emitted from gas orbiting the central mass at a greater radii. With the study of AGN and the variation in continuum luminosity and emission line flux, Peterson et al. (2004); Bentz et al. (2006) have measured variations that are a result of subarcsecond activity in the region of the supermassive black hole. Essentially, what is being observed is the fluctuations in the continuum emission caused by accretion onto the black hole accretion disk which, in time-of-flight, ionizes the broad-line region causing emission line flux variation from the broad line region. The time lag between these two events, given speed of light transmission of energy, gives the radius of the broad line region from the accretion disk. The radius of orbiting

material is a powerful component to the equation for measuring the mass of a gravitational host mass. The other half of the component is the speed at which the orbiting material is traveling, which can be extrapolated from the width of a broad emission line signature from the broad line region. Assuming a circular Keplerian virialized orbit around the SMBH, we now have the distance and speed at which the gasses orbit, by which, we calculate the mass of the SMBH at the center of these AGN or mass inside the virial orbit. Reverberation mapping is a telescope time intensive experiment and for distant AGN, which require larger telescopes, this becomes a costly task, for this reason a mass scaling relationship was created by (Peterson et al., 2004). This mass scaling relationship, for AGN broad line region radius, uses the continuum luminosity at a given wavelength as a proxy for the broad line region radius. This allows the radius to be extrapolated from a single epoch spectra, opposed to a complete reverberation mapping study which could take years (Vestergaard & Peterson, 2006).

1.5.4 Spiral Arm Pitch Angle

As the spiral galaxies have a qualitative classification system for describing their form, we are aimed at putting a quantitative system in place for the purposes here (Berrier et al., 2013). We do not let the bar of a galaxy change this quantity but we simply give an angle measure to the tightness of the spiral arms which are visible, starting from the center or the end of a bar. This angle is described as the angle between two tangent lines at the same point on the galaxy, one on the spiral arm and one on a circle with a radius of that chosen point. For this method we adopt the 2D FFT method described by Davis et al. (2012).

2 Sample Selection

Seigar et al. (2008) discovered a relationship between spiral arm pitch angle and central black hole mass using 27 local galaxies with independent black hole masses determined by either direct measurements or mass lower limits from the Eddington limit. This was followed up with a more detailed examination of these galaxies, and additional nearby galaxies with black hole mass estimates, by Berrier et al. (2013).

We identified 125 galaxies with spiral structure in the GOODS South field using HST optical images. Hasan (2007) provides morphological classifications to study the nature of the AGN host galaxies. We use Hasan (2007) paper titled "Morphologies of AGN Host Galaxies Using HST/ACS in the CDFS-GOODS Field" for AGN X-ray selection. Hasan (2007) gives 192 galaxies with which an HST/ACS optical image of a galaxy is classified as an AGN with information from a Chandra X-ray point source in the GOODS-S field. This sample was collected from the GOODS-S field using four bands from the Hubble Deep Field-South (HDF-S) and the Chandra Deep Field-South (CDF-S) (Hasan, 2007).

We also visually examined galaxies in the GOODS South field for galaxies that display extended morphology in the disk.

The two samples, 192 Hasan (2007) AGN and the 125 galaxies with extended morphology are cross-correlated.

Hasan (2007) studied the galaxies in order to make morphological classifications of the optical counterparts of the CDF-S X-ray point sources. The detection of a central X-ray point source suggests an AGN, the lack of an X-ray point source does not mean "no AGN," because the X-ray radiation could be obscured by an intervening gas and dust torus which absorbs the X-ray radiation (Treister et al., 2004).

From the GOODS-North field, 144 galaxies where visually identified as having possible spiral structure. Unlike in the GOODS-S field, we do not have a catalog of AGN galaxies in the GOODS-N field as Hasan (2007) provided for the GOODS-South field. AGN will exhibit an X-ray source unless it is heavily obscured (Treister et al., 2004). Alexander et al. (2003) published a catalog, "The Chandra Deep Field North Survey. XIII. 2 Ms Point-Source Catalogs" which covers an area of 448 arcmin^2 in the Hubble Deep Field-North (HDF-N). Using the X-ray point sources as proxies for AGN activity, we cross-correlated and found

GOODS-South AGN with Spiral Structure

HST Section.X.Y	RA	DEC	z	P $\pm error$	$M_{BH}(M_{\odot})$	Comments
12.6029.6234	03:32:52.8855	-27:51:19.832	1.22	12.1±0.1	3.3E07±6.8E6	Szokoly 15
22.0361.5312	03:32:47.1772	-27:51:47.545	1.114	33.8±1.6	7.4E5±1.5E5	No Szokoly
25.7031.0484	3:32:32.0726	-27:41:55.174	0.96	16.9±1.0	1.4E7±2.9E6	GOODS, No Szokoly
33.1645.1497	3:32:25.7412	-27:49:36.302	0.577	14.9±0	2.0E7±4.2E6	Szokoly 233
33.7627.8014	3:32:12.2214	-27:46:20.729	1.0314	18.7±1.9	1.0E7±2.2E6	No Szokoly, nearby object
34.6907.6883	3:32:13.8574	-27:42:48.911	0.735	29.8±1.3	1.5E06±3.1E5	X-Ray class. AGN-2, Szokoly 266
35.1313.3137	3:32:26.4961	-27:40:35.584	1.031	18.1±0.7	1.2E7±2.4E6	Szokoly 44a

Table 2.1: Here we present the 7 galaxies found in the GOODS-South field along with an initial spiral arm pitch angle measurement. The comments show the corresponding spectroscopic observation comments from Szokoly et al. (2004). Coordinates in J2000 and the Pitch angle in degrees.

that 23 of the 144 galaxies exhibiting spiral structure also emit an X-ray point source. The energy bins for X-ray strength are 0.3 keV - 1 keV, 1 keV - 2 keV, and 2 keV - 8 keV for soft, medium, and hard, respectively. In the GOODS-N field we identify AGN with spiral structure and conduct a search for corresponding spectra exhibiting broad emission lines.

These AGN identified as having spiral structure are then cross-correlated with the spectroscopic database Team Keck Redshift Survey (TKRS) (Wirth et al., 2004). These spectra are then visually inspected for the presence of a broad MgII emission line at λ_o 2798.06 Å. The broadening of the emission line is partially due to thermal broadening, but primarily caused by Doppler broadening due to the high orbital velocity of the ionized gas. After inspecting all 23 galaxies with spiral structure, one was identified as having spectra and also exhibiting a broad MgII emission line. This galaxy is identified in the spectroscopic catalog as TKRS3660.

2.1 The GOODS Fields

The Great Observatories Origins Deep Survey (GOODS) is comprised of observations across the electromagnetic spectrum from the National Aeronautics and Space Administration (NASA) as well as the European Space Agency (ESA), and ground and space based observatories (Alexander et al., 2003; Giavalisco et al., 2004; Wirth et al., 2004; Barger et al., 2008). The GOODS team selected two fields, one in the Northern hemisphere and one in the Southern hemisphere, as being ideal for deep observations, also taking the ground based observatory locations, such as Gemini, Keck, La Silla, Subaru, and ESO-VLT, into consideration. Space based observatories that gather data on these fields include HST, Chandra, Spitzer, ESA's Herschel, and XMM-Newton. Ground based observatories have also been used to gather spectroscopic data including Keck DEIMOS (Deep Imaging Multiobject Spectrograph) and ESO's VLT VIMOS (Visible Multiobject Spectrograph). We use archived observations of the Northern and Southern field known as the GOODS-South and GOODS-North. These two fields cover an area of about 320 square arc minutes on the sky. The initial observation of the Northern field was the Hubble Deep Field North (HDF-N). GOODS-N is center on the HDF-N at $12^h36^m55^s$, $+62°14^m14^s$ (Giavalisco et al., 2004). GOODS-S is centered on the J2000 WCS $03^h32^m30^s$, $-27°48^m20^s$ with an area of $30'$ x $30'$ (Giavalisco et al., 2004).

GOODS-North X-ray Point Sources with Spiral Structure

HST Section.X.Y	RA	DEC	z	$P \pm error$	$M_{BH}(M_{\odot})$	Comments
23.1649.1194	12:37:41.3740	62:12:51.618	1.6	25.9±0.5	3.0E6±6.1E5	TKRS 12640.18.40
23.6333.1046	12:37:21.2771	62:12:47.508	0.104	15.0±0.3	2.0E7±4.1E6	TKRS 10574.16.70
24.2036.1347	12:37:39.8172	62:17:02.001	0.458	19.6±0.3	8.9E6±1.8E6	TKRS 8760.14.100
32.1733.7452	12:37:05.8615	62:11:54.057	0.9032	33.7±0.0	7.6E5±1.6E5	TKRS 9727.14.55
33.1275.7660	12:37:07.8555	62:16:06.047	0.936	18.1±0.2	1.2E7±2.4E6	TKRS 6303.9.71
33.2467.6923	12:37:02.7307	62:15:43.961	0.51236	28.9±0.6	1.8E6±3.6E5	TKRS 6082.9.68
33.6837.1142	12:36:43.9696	62:12:50.518	0.557	25.2±0.0	3.4E6±6.9E5	TKRS 6734.8.43
34.2027.1004	12:37:04.6275	62:16:52.143	0.37657	22.9±0.8	5.0E6±1.0E6	TKRS 5379.8.72
34.5601.4893	12:36:49.2539	62:18:48.827	0.593	33.7±0.0	7.6±1.6E5	TKRS 2255.2.80
41.2173.4390	12:36:28.9276	62:06:16.314	1.264	13.9±0.4	2.4E7±5.0E6	TKRS 10836.17.2
44.0748.0220	12:36:34.8641	62:16:28.555	0.847	24.6±0.4	3.7E6±7.7E5	TKRS 2812.3.61
52.1048.5773	12:35:58.5697	62:11:03.001	0.637	33.8±1.6	7.40E5±1.5E5	TKRS 3829
52.2323.4930	12:35:53.1194	62:10:37.566	1.379	16.2±0.2	1.6E7±3.3E6	TKRS 3660.5.3

Table 2.2: Here we present the 13 galaxies found in the GOODS-North field along with an initial spiral arm pitch angle measurement. Unlike the South field, these spiral galaxies where not classified as AGN and we therefor made a candidate AGN list based on X-ray point source observations. The comments show the corresponding spectroscopic observation comments from Wirth et al. (2004).

Observation Data

Field Source	RA	DEC	Redshift Range	# of Galaxies	# of AGN	# of Spirals
GOODS-South	$03^h32^m30^s$	$-27°48^m20^s$	z < 1.3	...	192	125
GOODS-North	$12^h36^m55^s$	$+62°14^m14^s$	z < 1.5	1440	...	144

Table 2.3: Location of Sample Data used

2.2 Optical

Imaging data comes from the HST advanced camera for surveys (ACS) optical and near infrared imaging in 4 bands (F435W, F606W, F814W, and F850LP) ($B_{435}, V_{606}, i_{775}, z_{,850}$) of the GOODS fields (Giavalisco et al., 2004). The Hubble Space Telescope (HST) is in a low Earth orbit in order to bypass the atmosphere when viewing from the near-infrared to ultraviolet wavelengths of light with its 2.4 meter primary mirror. HST was launched aboard the space shuttle Discovery on the 24th of April 1990. The GOODS team was awarded 398 orbits with the HST/ACS in order to observe the North and South fields (Giavalisco et al., 2004). B_{435}-band images were taken initially and then the other band images were taken with 40-50 days between to increase the search for distant supernovae (Giavalisco et al., 2004). An area of about $10' \times 16'$ is common among all GOODS observations (Giavalisco et al., 2004).

The images are available on the STScI MAST HST/ACS GOODS data archive[1], listed by section number and (x, y) coordinates.

We collected the images of the galaxies from the GOODS archive and made cutouts of the individual galaxies with which we de-projected each band image. These images were collected and a cut-out was created for each galaxy using IRAF `imcopy` command. After acquiring the archived HST imaging data from the Space Telescope Science Institute (STScI), we began a search for candidate spiral galaxies for which we could measure a spiral arm pitch angle. In this search we visually inspected the galaxies for evidence of a defined structure protruding from the central nucleus of the galaxy. We also investigated evidence for bars and halos. Any galaxy that exhibited a structure protruding from the central region, we marked as being a candidate for spiral structure. Visual inspection of the galaxies show spiral structure in each band image, with some band images showing more visible spiral structure than others.

These images were then used to measure the spiral arm pitch angle using a two-dimensional fast Fourier Transform (2DFFT) (Davis et al., 2012).

[1] www.archive.stsci.edu/prepds/goods/

2.3 Selection of Active Galactic Nuclei

The Chandra X-ray Observatory (CXO) was launched aboard space shuttle Columbia STS-93 on the 23rd of July 1999 as one of NASA's Great Observatories joining HST and the Compton Gamma-Ray Observatory (CGRO) (Weisskopf et al., 2000). The Chandra X-ray Observatory uses the Advanced CCD Imaging Spectrometer (ACIS) to locate the point sources (Garmire et al., 2003). The center point of the CDF-S (J2000 $3^h32^m28^s$, $-27°48^m30^s$) was selected for its low HI column density ($N_H = 8 \times 10^{19}$ cm^{-2}) in order to maximize the depth at low energies with optimal visibility of this field in Chile at ESO's observation site from September through January and no stars brighter than $m_v = 14$ (Giacconi et al., 2001).

The Chandra imaging X-ray band ranges from $0.08 - 10$ keV ($15 - 0.12$ nm) and display sub-arcsecond resolution (Weisskopf et al., 2000). The energy bins for X-ray strength are 0.3 keV - 1 keV, 1 keV - 2 keV, and 2 keV - 8 keV for soft, medium and hard, respectively. A signature of AGN, being high energy emission where a supermassive black hole is believed to power the high energy emission of X-rays from a small area, makes observations from Chandra ideal for locating AGN for this study.

The initial observation of the GOODS-South field was the Chandra Deep Field South (CDF-S) X-ray observation acquired with the Chandra X-ray Observatories Advanced CCD Imaging Spectrometer (ACIS) (Giacconi et al., 2001). The CDF-S master catalogue is a compilation of GOODS/CDF-S spectroscopy observed of optical counterparts to the Chandra point sources.[2] The GOODS-S field is centered at J2000 $03^h32^m30^s$, $-27°48^m20^s$ (Giavalisco et al., 2004). The initial X-ray sources detected in the CDF-S observation appeared to be obscured and unobscured AGN (Giacconi et al., 2001). Hasan (2007) finds 192 optical counterparts for the Alexander et al. (2003) Chandra X-ray point sources in the CDF-S. Our goal is to find galaxy candidates which have a spiral structure and an active nuclear region exhibiting broad lines. For location coordinates in the STScI HST database, a galaxy ID or coordinate indicator identifies the galaxies section number, x-axis coordinate, and y-axis coordinate. Hasan (2007) lists the galaxies, not by their right ascension and declination but by their section number and X and Y coordinate within that section.

The 144 candidate spiral galaxies in the North field were cross correlated with the Alexander et al. (2003) X-ray point source catalogue and 23 of the spiral candidates exhibited an

[2] www.eso.org/sci/activities/garching/projects/goods/spectroscopy.html

X-ray point source.

A search revealed 20 galaxies from GOODS-N with archived spectroscopic observations from the Team Keck Redshift Survey (TKRS) and 5 galaxies from GOODS-S had archived spectra from ESO VLT VIMOS and FORS 1 & 2 (Szokoly et al., 2004).

2.4 Spectroscopy

Spectroscopic observations were carried out throughout the spectrum in both the GOODS North and South fields. After collecting the RA and Dec for each galaxy, a cross correlation search was carried out using the VLT/FORS2 spectroscopy master catalog (Szokoly et al., 2004).[3] Searches were carried out using the NASA/IPAC Extragalactic Database (NED) to locate spectra for these object.

The GOODS-South spectra covers optical to NIR and was carried out using the FORS2 instrument mounted at the Kueyen, Unit Telescope 2, of the VLT at ESO's Cerro Paranal Observatory, Chile (Szokoly et al., 2004). Szokoly et al. (2004) gathered spectroscopic data for 251 of the 349 X-ray point sources observed by Chandra X-ray observatory in a 942 ks exposure of the Chandra Deep Field-South. The FORS surveys uses a $1''$ wide slit with a range of 6000Å to 10000Å and 3.2Å per pixel. Note that these AGN have not been confirmed as exhibiting broad lines for the mass scaling relationship. Szokoly et al. (2004) published optical spectroscopy for the GOODS-South field in the range of $4000\text{Å} \geq \lambda \geq 8000\text{Å}$ which places MgII redshift at $0.5 \geq z \geq 1.8$. Seven galaxies were selected for further investigation. Of the 7 AGN, spectroscopic data is available for 6 and a broad line is shown in two, with one having good (2.0+) data quality and the other having (1.0) data quality indicating "a reliable redshift determination" and "clearly detect some feature (typically a single narrow emission line) in the spectrum that can not be identified securely" respectively (Szokoly et al., 2004). The Szokoly et al. (2004) spectroscopic survey was intended to be an exploratory survey, therefore the spectra has a low signal-to-noise quality and can be used to setup more directed observations in the future. Two galaxies from this sample show spiral structure that can be measured with the spiral arm pitch angle method and a broad MgII emission line.

The Team Keck Redshift Survey (TKRS) collected spectra of 1440 galaxies in the GOODS-North field using DEIMOS on the Keck II 10 meter telescope (Wirth et al., 2004).

[3] http://www.stecf.org/goods/spectroscopy/CDFS_Mastercat/

Broad Line Active Galactic Nuclei with Spiral Structure			
GOODS ID	z	$P \pm error$	Comments
J033252.89-275119.9	1.227	-10.3 ± 1.0	Szokoly 15
J033226.49-274035.6	1.031	$+37.7 \pm 7.1$	Szokoly 44a
J123553.12+621037.5	1.371	$+26.7 \pm 6.2$	TKRS 3660

Table 2.4: Column 1: GOODS Object Name. Column 2: Spectroscopic Redshift. Column 3: Spiral Arm Pitch Angle with Error. Column 4: Spectroscopic Survey Object Name

Cowie et al. (2004) observed at Keck II DEIMOS spectrometer January 2003 - January 2004 with 600 lines mm^{-1} grating, resolution of 3.5Å with wavelength coverage of 5300Å and covers an area of 160 arc min^2 in the HDF-N. Cowie et al. (2004) spectroscopic data is a part of the Team Keck Redshift Survey (TKRS) and observations where carried out on the Keck II DEIMOS spectrometer from January 2003 to January 2004 with a 600 lines mm^{-1} grating, resolution of 3.5Å with wavelength coverage of 5300Å centered at 7200Å, although each λ range for each spectrum depends on the slit position. Wirth et al. (2004) also carried out some of the Team Keck Redshift Survey over the same range and resolution. Of these 23 galaxies, 20 were observed spectroscopically by Cowie et al. (2004). Galaxy ID 35.1314.3138 at a redshift of 1.031 is classified as an interacting galaxy and ID 12.6029.6234 at a redshift of 1.22 is classified as Sab (Hasan, 2007).

In order to confirm these masses, using a mass scaling relationship (McLure & Jarvis, 2002; Vestergaard & Peterson, 2006), we must also find spectroscopic data for these AGN that captures a broad emission line Mg II or C IV line and can have the continuum luminosity measured at 3000Å or 5100Å, respectively.

After a visual inspection of the spectra available, we found two in the South and one in the North which displayed a broad MgII emission line, $\lambda_0 = 2800$Å. Here we exploit the measurement of the MgII line with $\lambda_\circ = 2798$Å in order to use the mass scaling relationship of McLure & Jarvis (2002); McGill et al. (2008). With these galaxies located at $z \simeq 1$, the MgII emission line is shifted into the visible at $\lambda \simeq 5600$Å.

3 Analysis

3.1 Measuring Pitch Angle

We adopt the technique for measuring the pitch angle of the spiral arm from Davis et al. (2012).

In order to measure the pitch angle of the galaxy we first deproject the image to be face-on, assuming that the galaxies are circular. The `.fits` image is then converted into a text file, with `wtextimage`, in order to operate a 2 dimensional fast Fourier transform (2DFFT). The transform finds the periodicity in the spiral structure according to the intensity of each pixel. This in turn gives a pitch angle for which the spiral arms are loose, giving a greater angle and tight giving a lesser angle. For this reason, we run the 2DFFT script at each varied inner radius with a fixed outer radius. Barred spiral galaxies are more challenging in that the inner radius at which the spiral stops and the bar begins is obscured by the bar. Two tests have been carried out in which we vary the inner radius about its entire length from the center to the outer radius and we vary the deprojection angle, meaning the circularity of the galaxy. In this test, it is determined that the deprojection, varying the angle at which the galaxy is viewed, does not change the spiral arm pitch angle by more than error allows.

Of the three galaxies, two are from the GOODS-S field and one from the GOODS-N field. Here, the galaxies are referred to as Szokoly 15, Szokoly 44a and TRKS 3660 respectively using there spectral identification. These names are given by the spectroscopic surveys which obtained spectra for these galaxies and the GOODS names are J033252.89-275119.9, J033226.49-274035.6 and J123553.12+621037.5.

For each of the galaxies, a spiral arm pitch angle is measured for two variables; 1 to 6 arms, and for each arm a different inner radius, in polar coordinates, from 0 to the outer radius at the edge of the visible disk and these results are used to find an average and an error. From this information a plot is created with inner radius vs. pitch angle for each mode, 1 through 6 of the number of spiral arms. A concern that requires further attention is how the center of the galaxy is determined. For these AGN, the central region is very bright and spherical so it looks circular at any inclination angle. With the central nuclear region being so bright, the galaxy may be off-center in the final de-projected image. Further test

of the significance of this uncertainty and its effect on the calculated spiral arm pitch angle show that the offset of the center does not significantly change the P measurement within error.

We have performed a test as to whether the deprojection angle stabilizes the pitch angle vs. inner radii plot. In this test we take the three low resolution AGN and create 10 different deprojections from no deprojection ellipticity of 0 to assuming an ellipticity of 0.474 or x-axis magnification of 1 to 1.9, respectively. For each image, the original position angle from the previous measurements is used.

The spiral structure may not be discernible, due to the edge-on orientation of the galaxy, the spiral galaxy is flocculent, tightly wound and the arms are buried in the bulge, AGN with high bulge luminosity to total luminosity (B/T) luminosity out-shines the disk of the galaxy, or simply too far away for the telescope to resolve the spiral structure.

3.1.1 Szokoly 15

Szokoly 15 is located in the Southern hemisphere GOODS field and appears to be a barred spiral with two arms, but this is only obvious after the de-projection is preformed. Hasan (2007) describes this galaxy as an "elliptical galaxy with star formation taking place along a ring on the disc" although, with a bulge luminosity to total luminosity ratio (B/T) in the i band of 0.50 and $\chi^2 = 1.25$, the galaxy is given a morphological type Sab. Szokoly 15, b-band image, gave a position angle of $-35.33°$ and an ellipticity of 0.466. The final de-projected image was 140×140 pixels with the center of the galaxy, measured with IRAF `imcntr`, at the center of the image. The de-projected image showed a barred spiral with two arms rotating in a counter-clockwise direction. Visual inspection showed the arm to be located at a radius of 15 to 30 pixels from center. Pitch angles where measured out to a radius of 70 pixels. The b-band 2DFFT nominal pitch angle for the 2 arm mode is located in the R vs. P plot from a radius of 15 to 30, giving an angle of $+9.55 \pm 3.75°$. The image could also be interpreted as having only one arm that looks like a halo around the central region, which is congruent with the R vs. P plots, as the 1 arm mode is most stable from 10 to 35 pixel radius. The one arm interpretation is stable for approximately $-10°$ and the two arm and one arm match for approximately $+10°$ from 35 to 40 pixel radii. The two arm region is stable from 25 to 40 pixel radii, afterwards the angle approaches 2° out to a radius of 65 pixels. The 2 arm mode is not stable in the v i and z band 2DFFT. The dimming of the

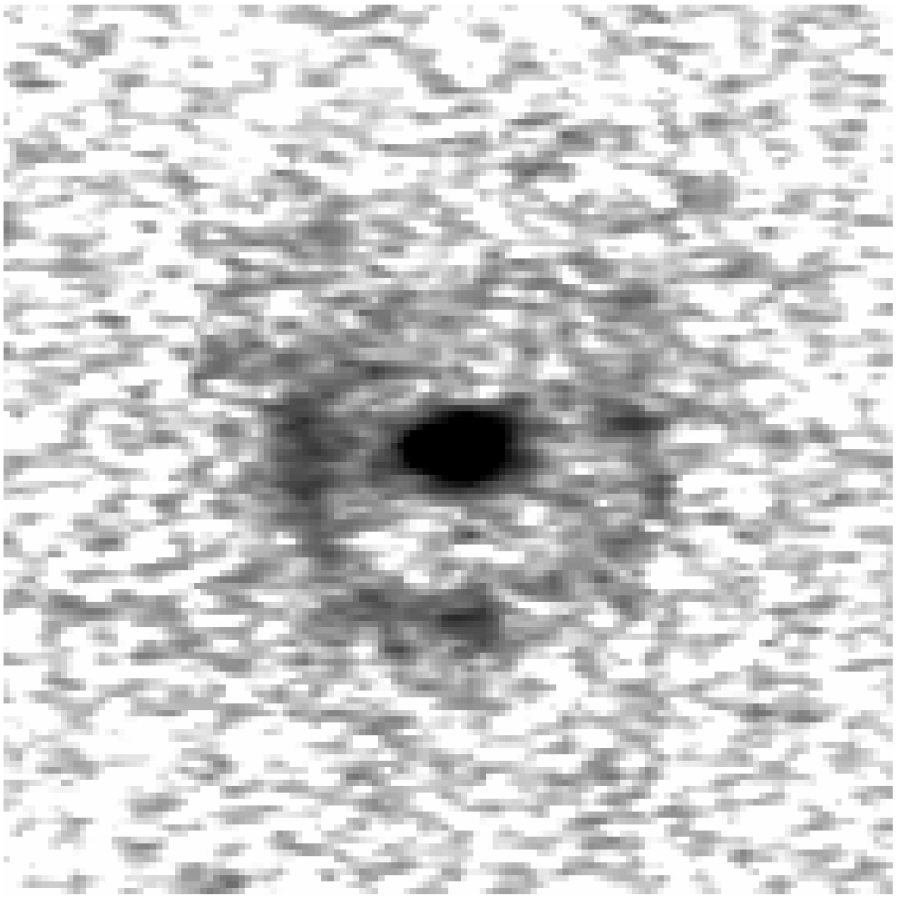

Figure 3.1: Szokoly 15 b-band De-projection

second arm could be due to the inclination angle causing an obscuration of photons which have a greater distance to travel from the far side through the gas and dust halo around the galaxy. Consistent over all four bands is the one arm mode at 10 to 25 pixel radii around -10° pitch angle and then after this radius it becomes stable again at $+10^\circ$ from 40 to 45 pixel radii. The visible spiral structure, though difficult to guarantee, is from 15 to 35 pixel radii, so the overlapping stable region for both is 15 to 25 pixel radii. This mode averages over all four bands gives -10.29 ± 0.94

3.1.2 Szokoly 44a

Szokoly 44a is located in the Southern hemisphere GOODS field and appears to be a two armed spiral AGN. Hasan (2007) describes this galaxy as a "spiral Sb galaxy (or long arm created out of interaction) with a nearby object also showing star formation along the disc closer to the galaxy which shows star formation on the complete disc" and calculates

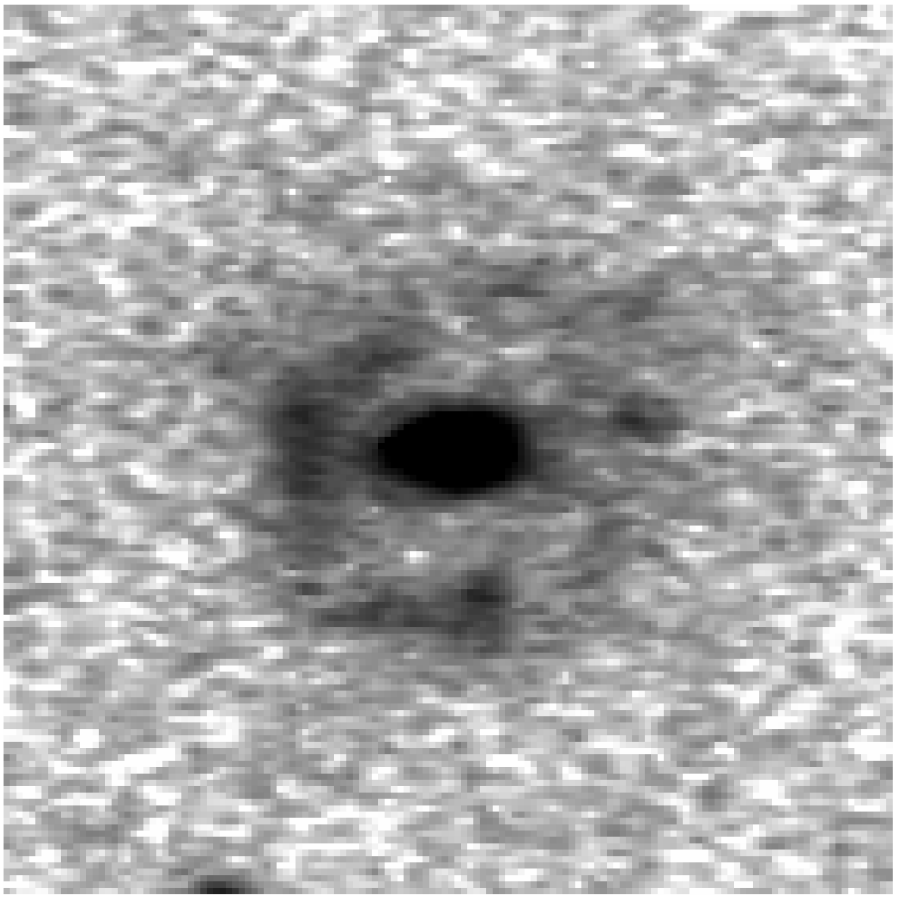

Figure 3.2: Szokoly 15 v-band De-projection

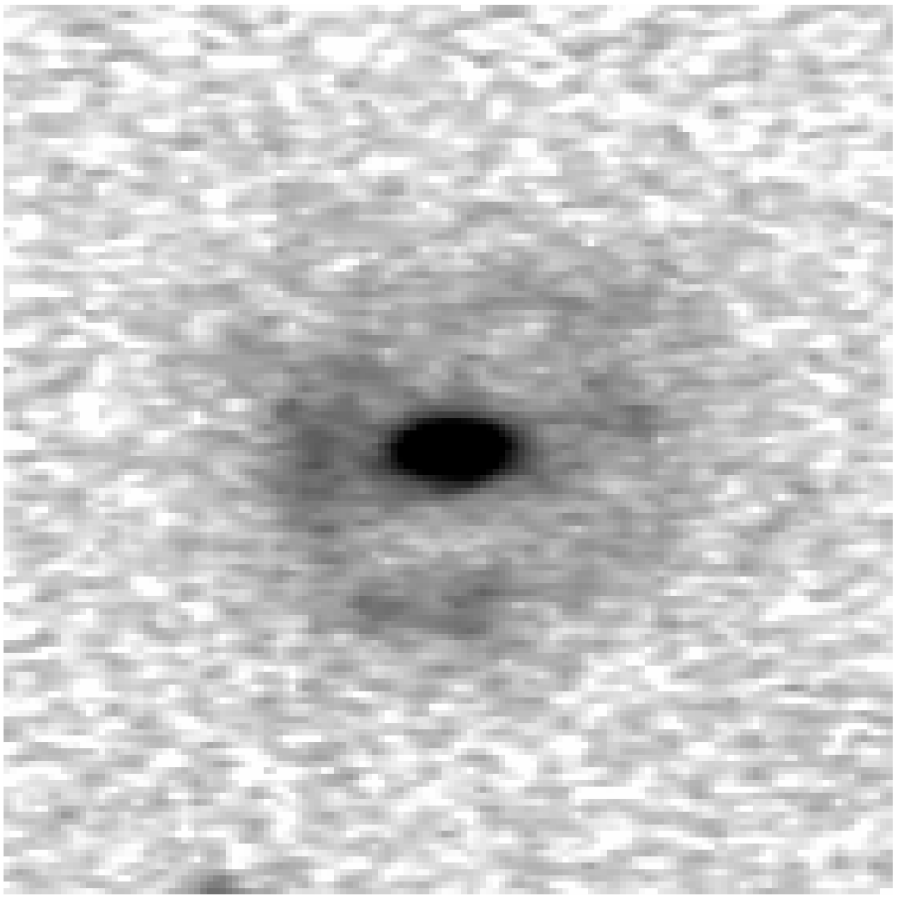

Figure 3.3: Szokoly 15 i-band De-projection

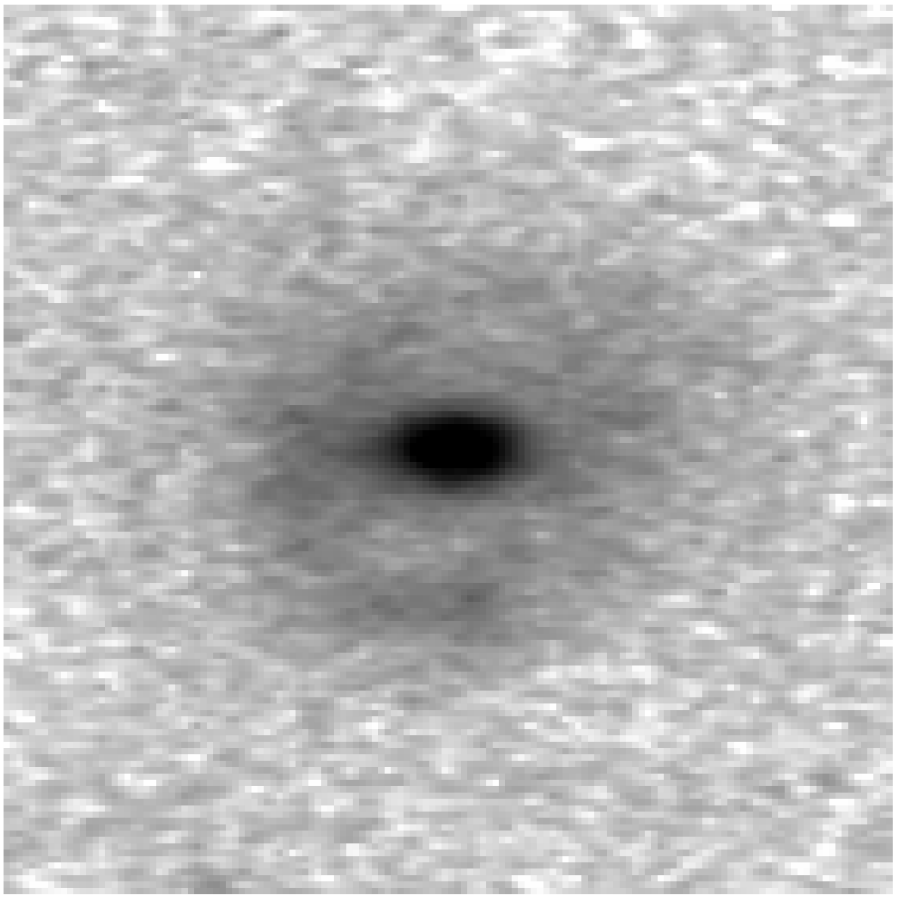

Figure 3.4: Szokoly 15 z-band De-projection

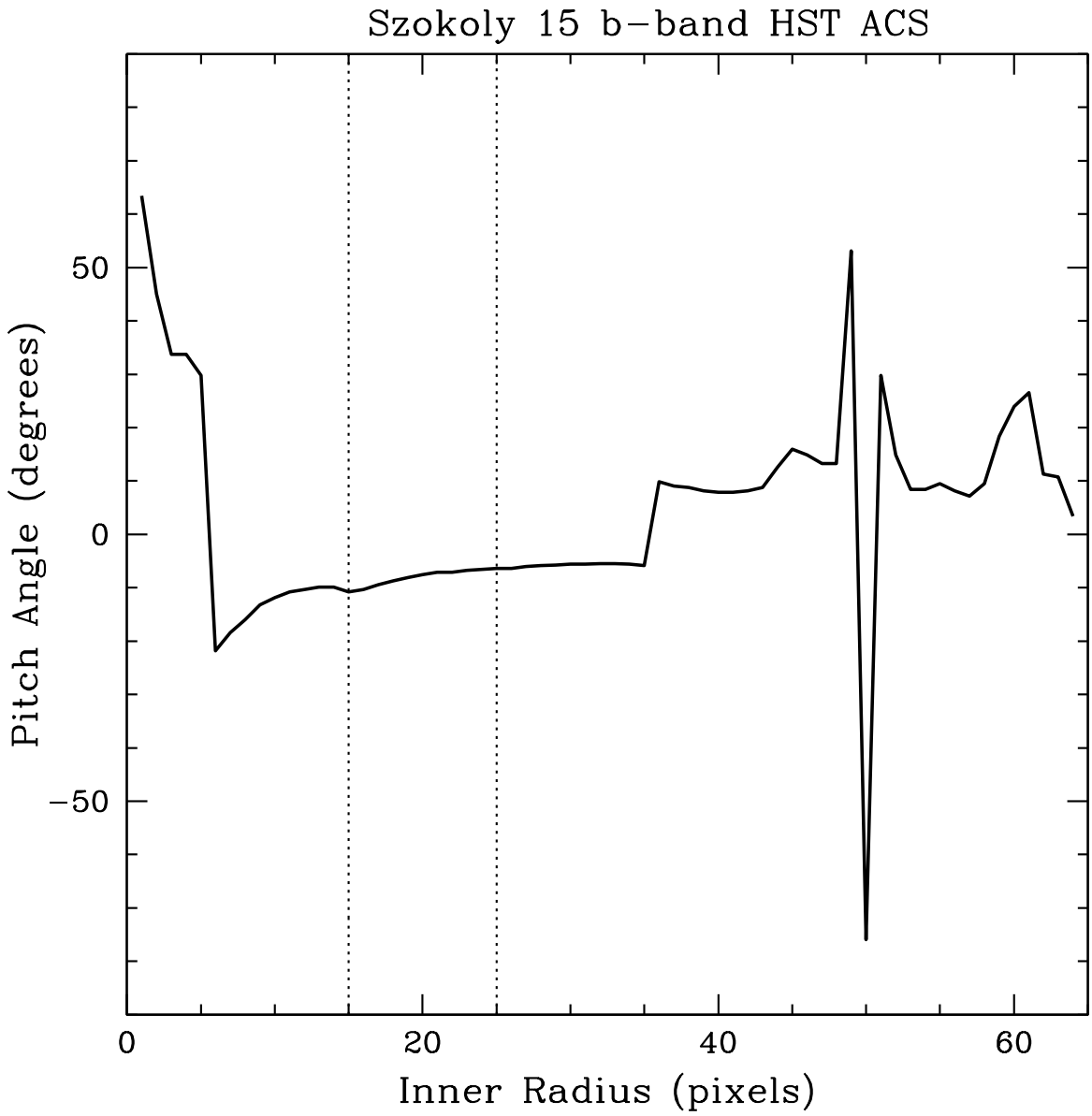

Figure 3.5: Inner Radius vs. Pitch Angle Szokoly 15 b-band

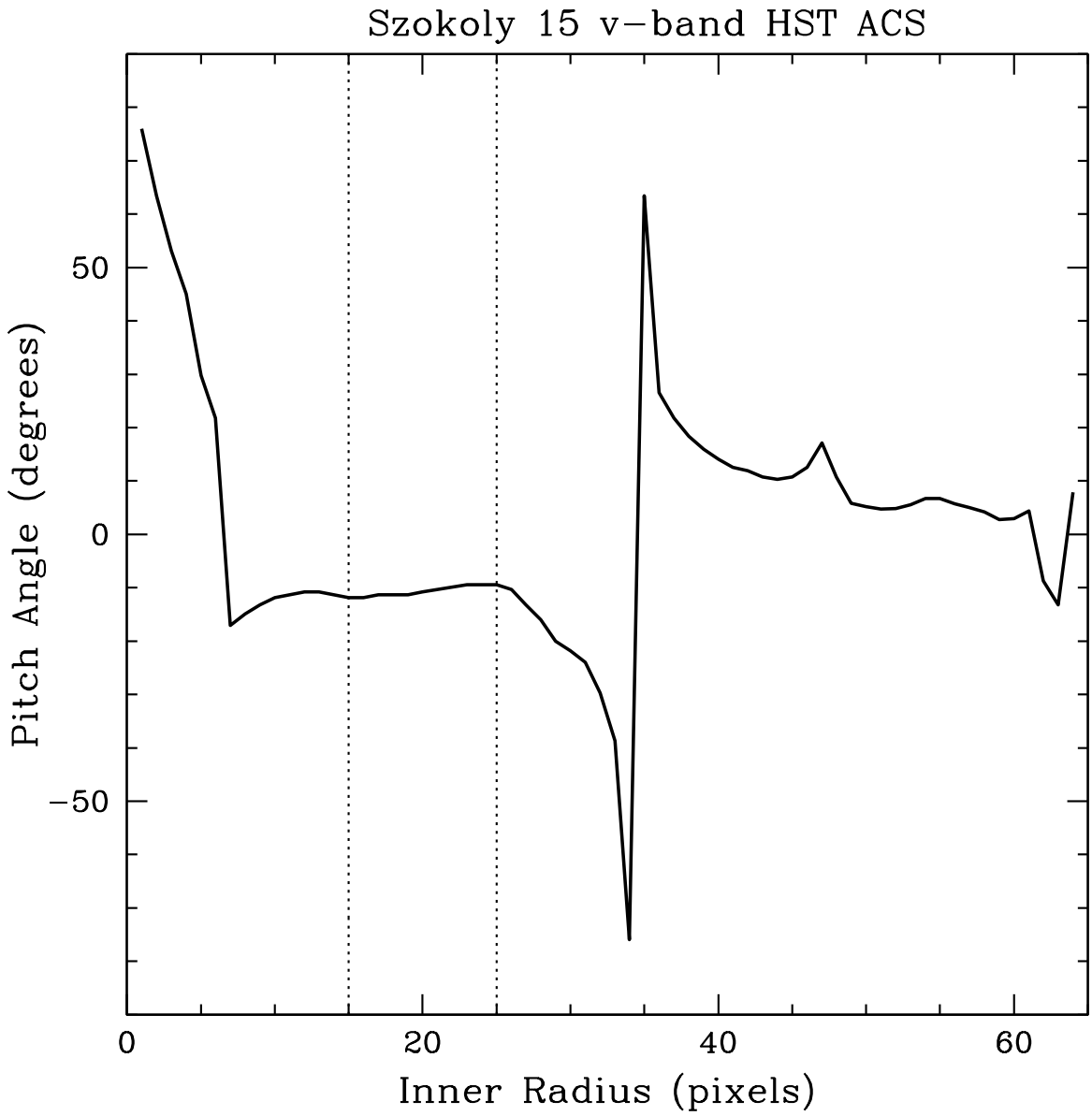

Figure 3.6: Inner Radius vs. Pitch Angle Szokoly 15 v-band

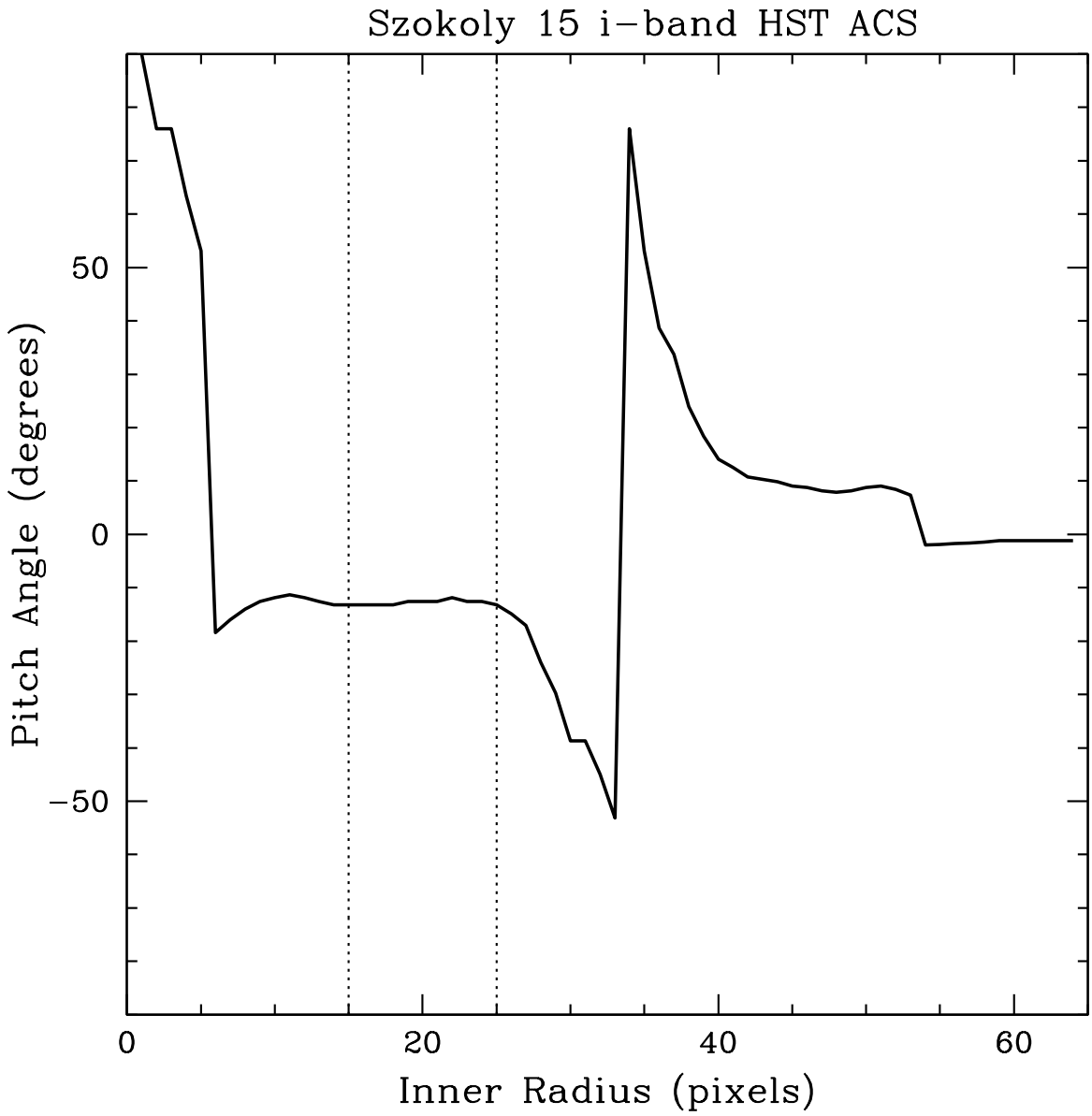

Figure 3.7: Inner Radius vs. Pitch Angle Szokoly 15 i-band

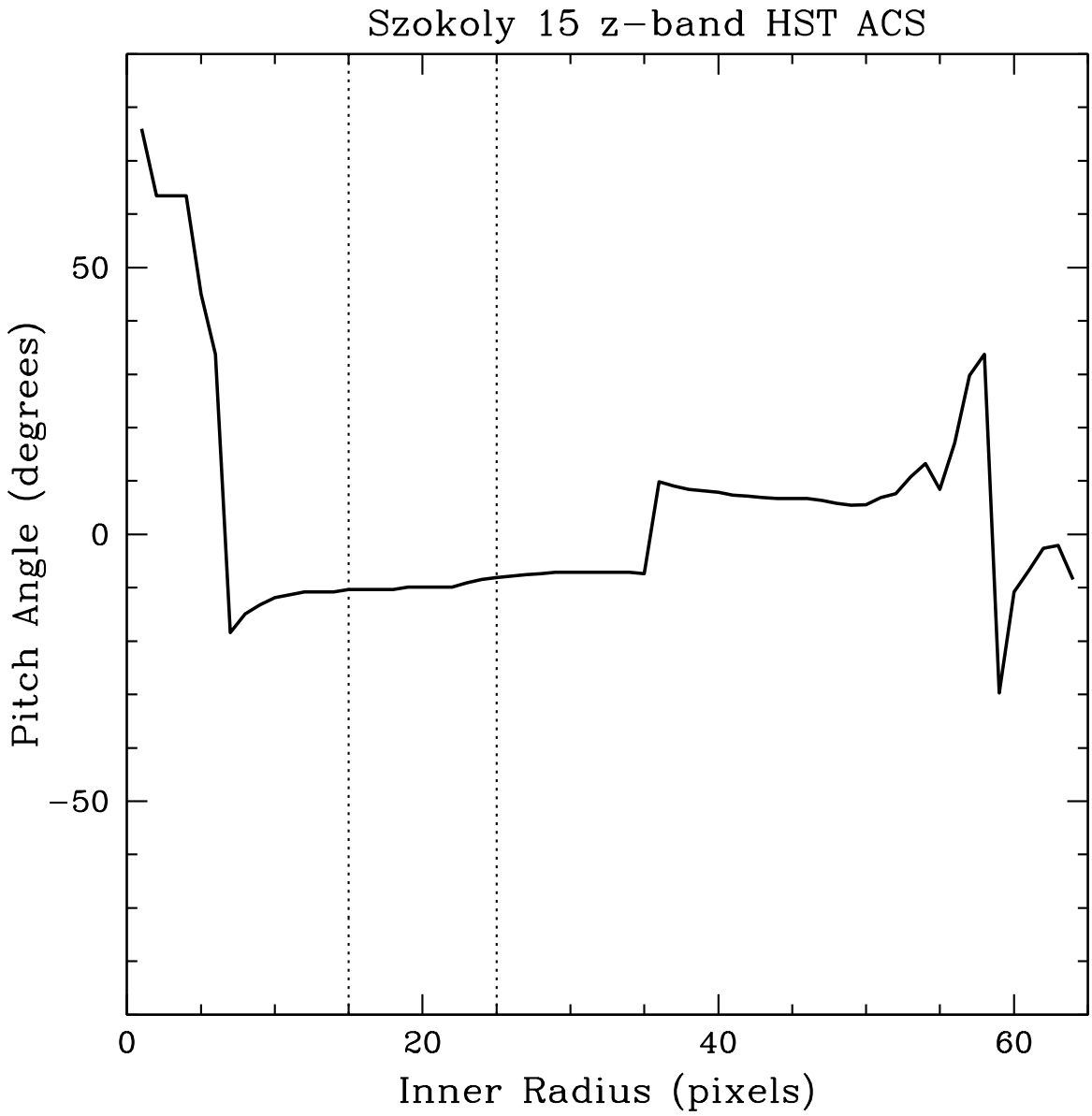

Figure 3.8: Inner Radius vs. Pitch Angle Szokoly 15 z-band

a B/T ratio in the i band of 0.52 with $\chi^2 = 12.96$. Visual inspection of the de-projected image shows a one or two armed spiral galaxy rotating clockwise.

The `ellipse` task in IRAF was used to fit Szokoly 44a b-band image and gave a position angle of $-76.12°$ and an ellipticity of 0.417.

These two quantities where used to de-project each of the 4 band images. The final de-projected image, with which a 2D FFT was ran, measured 160×160 pixels. Pitch angles where measured out to a radius of 70 pixels. With the extended features of this galaxy being difficult to detect visually, we look to the 2DFFT radius vs. spiral arm pitch angle for a consistent measure across all 4 bands and find a radius from 30 to 50 pixels to give $37.69 \pm 7.11°$. The one arm mode is stable across b, v, and i band at $-10°$ and in the z band at $-40°$ with an inner radius of 35 to 40 pixel radii for all bands. Also in the z band, we have convergence of modes $2-6$ at inner radius $35-40$ pixel radii at a pitch angle of $+45°$.

For this particular galaxy, this is a concern because it appears the galaxy is inclined on the opposite axis from visual inspection.

3.1.3 TKRS 3660

This galaxy is particularly difficult to measure a spiral arm pitch angle, due to the intermittent arm visibility. The galaxy appears to be a barred spiral with two arms and radially varying areas in the two arms with active star formation. Initially the plot seems to be most stable at the original image without any de-projection. This may be correct, seeing that from the original measurement of this galaxy we used a de-projection of ellipticity 0.165 or x-axis magnification 1.2 times. TKRS 3660 v band image showed the galaxy to have a position angle of $-86.82°$ and an ellipticity of 0.165. The de-projected image measured 80×80 pixels and the 2D FFT was operated out to a radius of 37 pixels. Visual inspection of the de-projected image showed a barred spiral with two arms rotating in the clockwise (+) direction and the arms located at a radius of 15 to 30 pixels from center. Nominal two mode pitch angle was located at 10 to 17 pixels from center giving a pitch angle of $26.7 \pm 6.2°$ averaged over all 4 bands. There is a discontinuity at a pixel radius of 20 in all four bands for the two mode measurement where the pitch angle goes from positive to negative. In the b band R vs. P plot the one mode line has the same discontinuity but opposite sign.

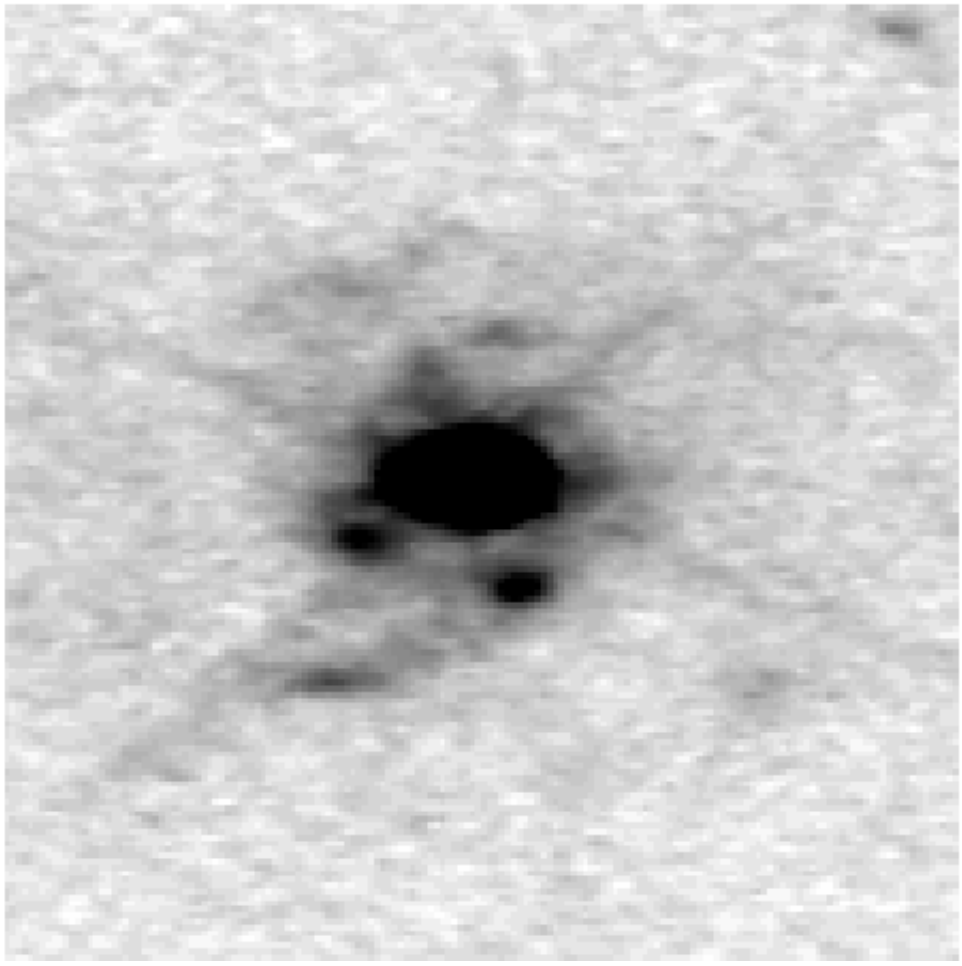

Figure 3.9: Szokoly 44a b-band De-projection

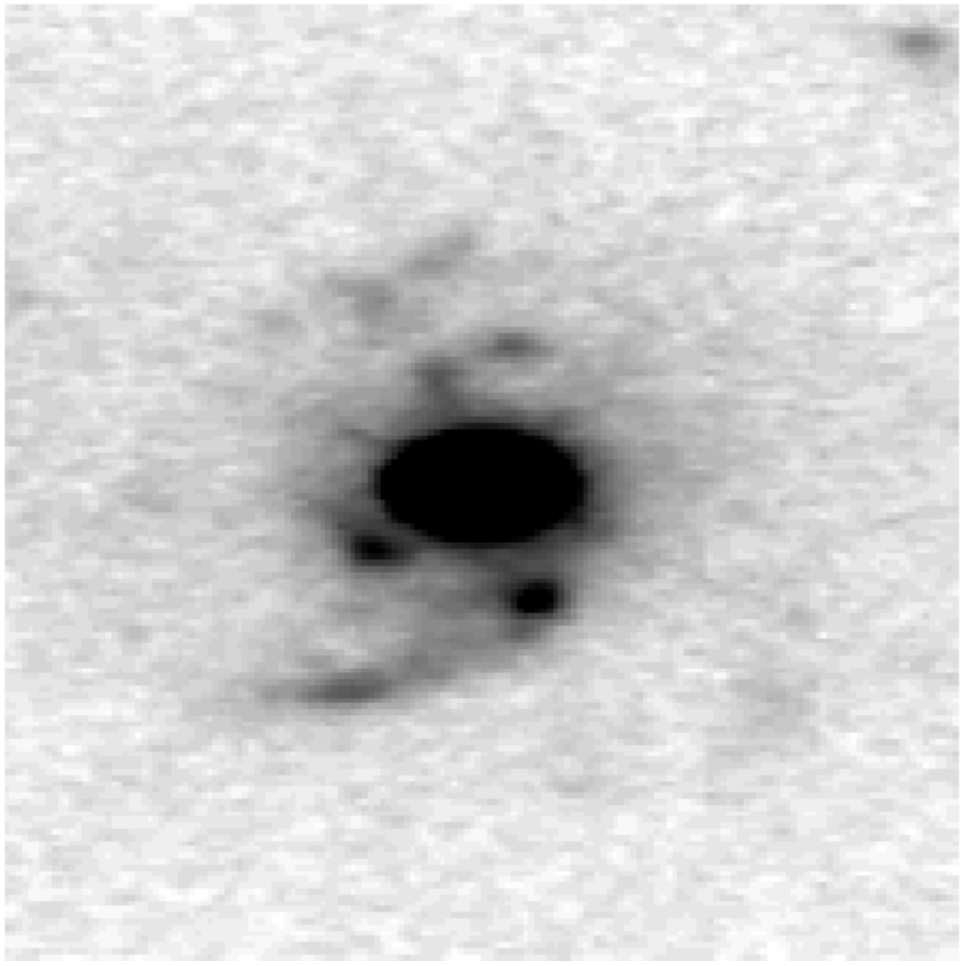

Figure 3.10: Szokoly 44a v-band De-projection

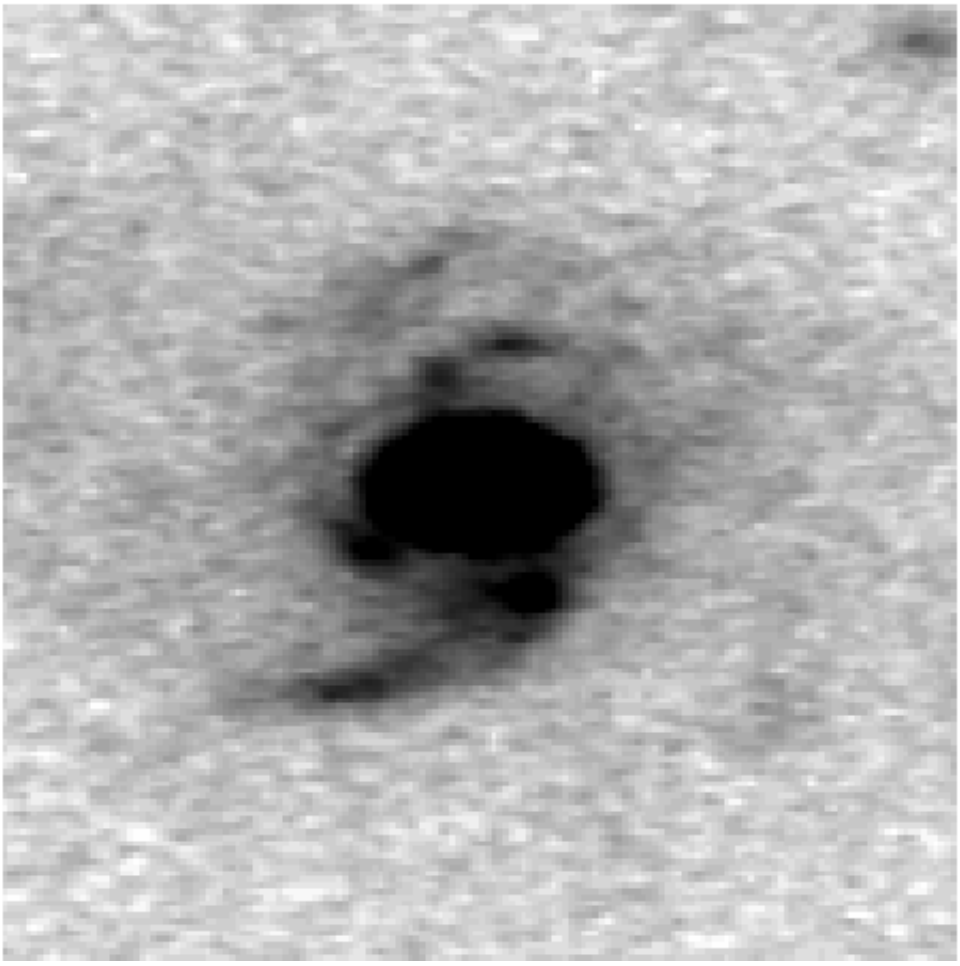

Figure 3.11: Szokoly 44a i-band De-projection

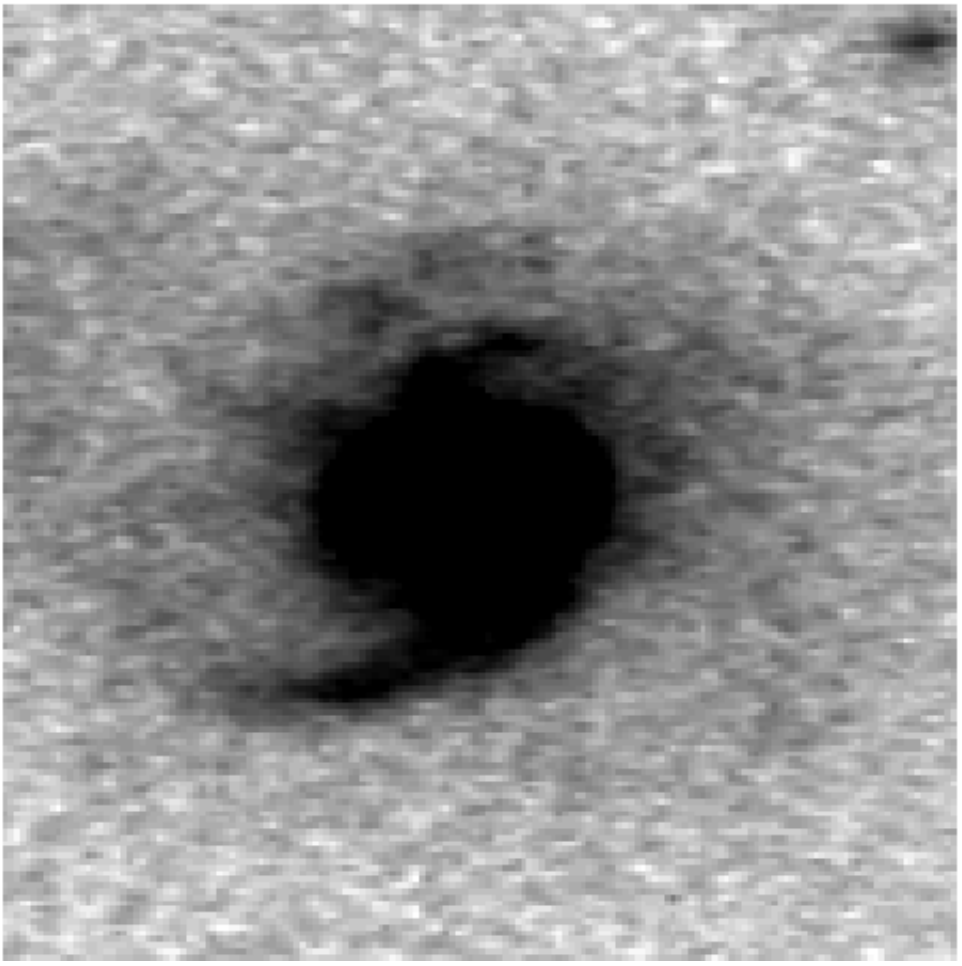

Figure 3.12: Szokoly 44a z-band De-projection

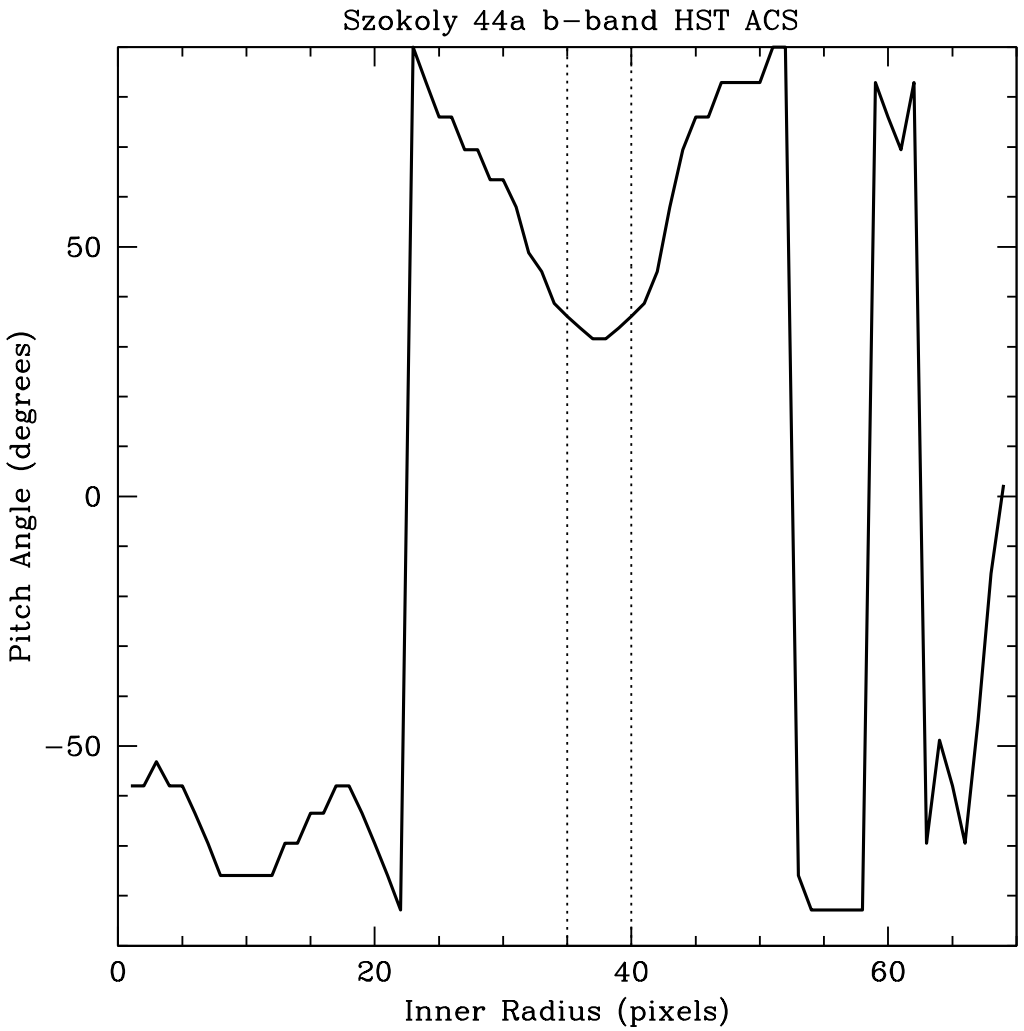

Figure 3.13: Inner Radius vs. Pitch Angle Szokoly 44a b-band

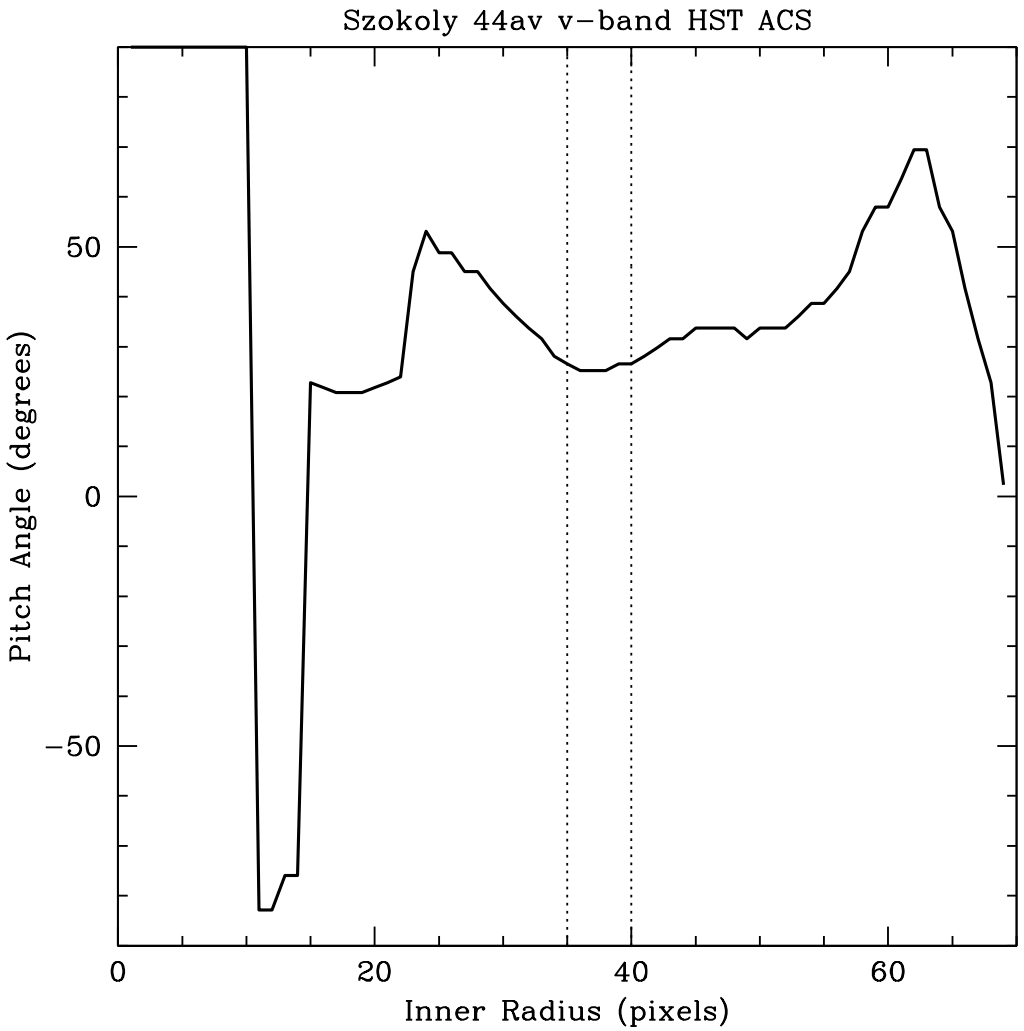

Figure 3.14: Inner Radius vs. Pitch Angle Szokoly 44a v-band

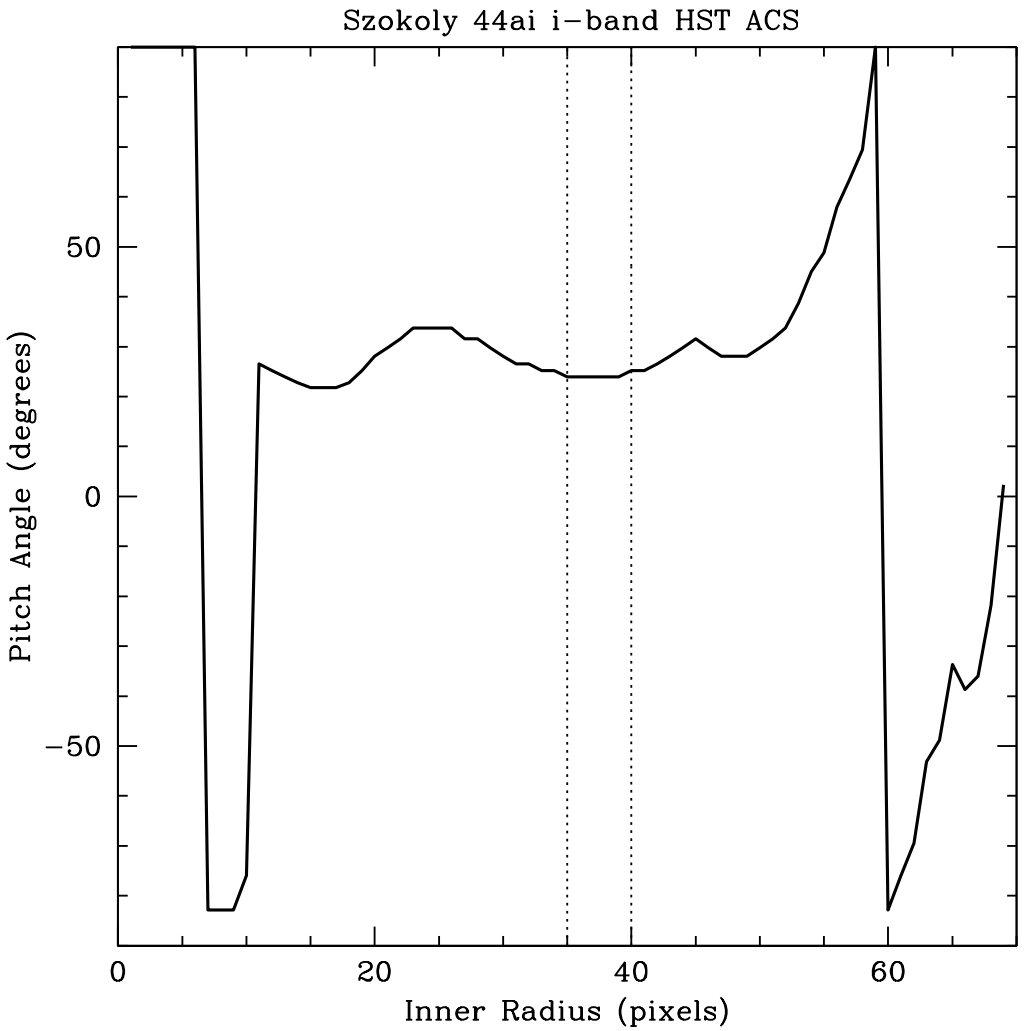

Figure 3.15: Inner Radius vs. Pitch Angle Szokoly 44a i-band

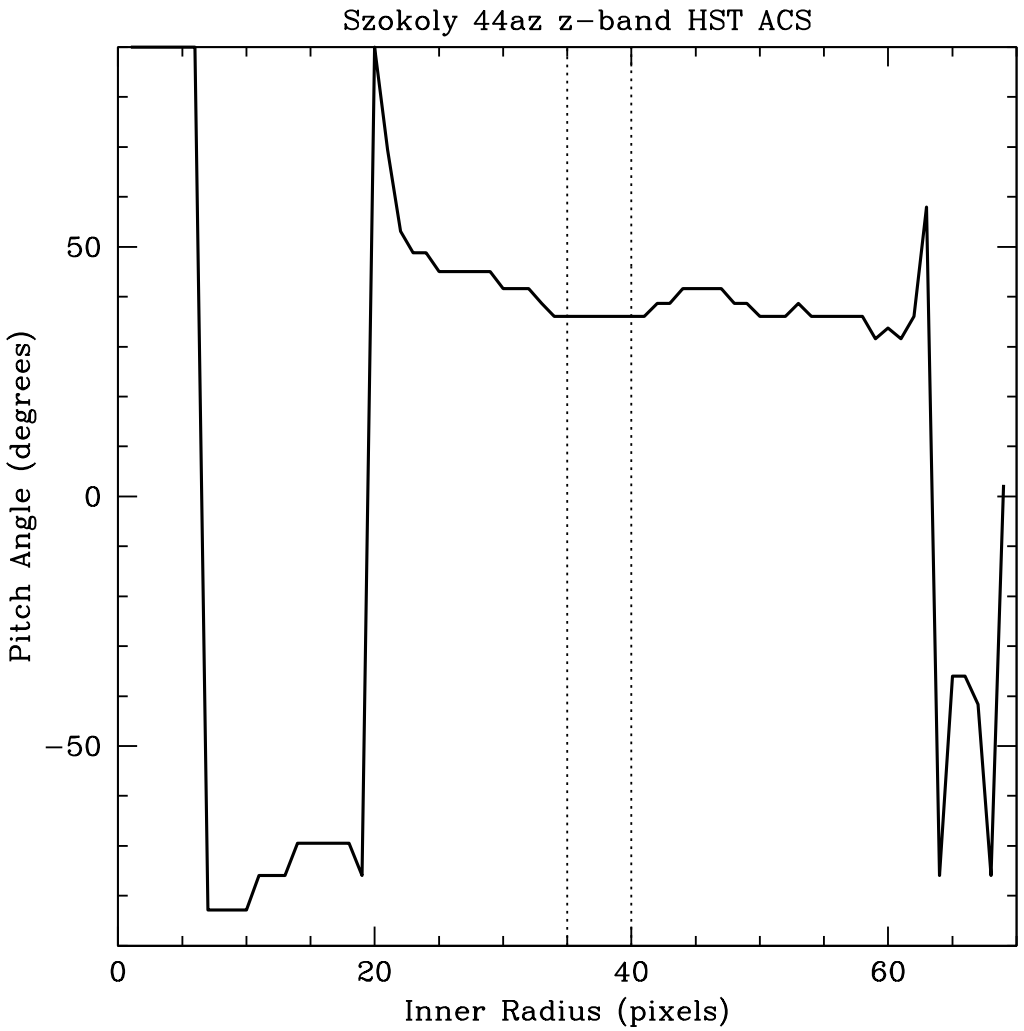

Figure 3.16: Inner Radius vs. Pitch Angle Szokoly 44a z-band

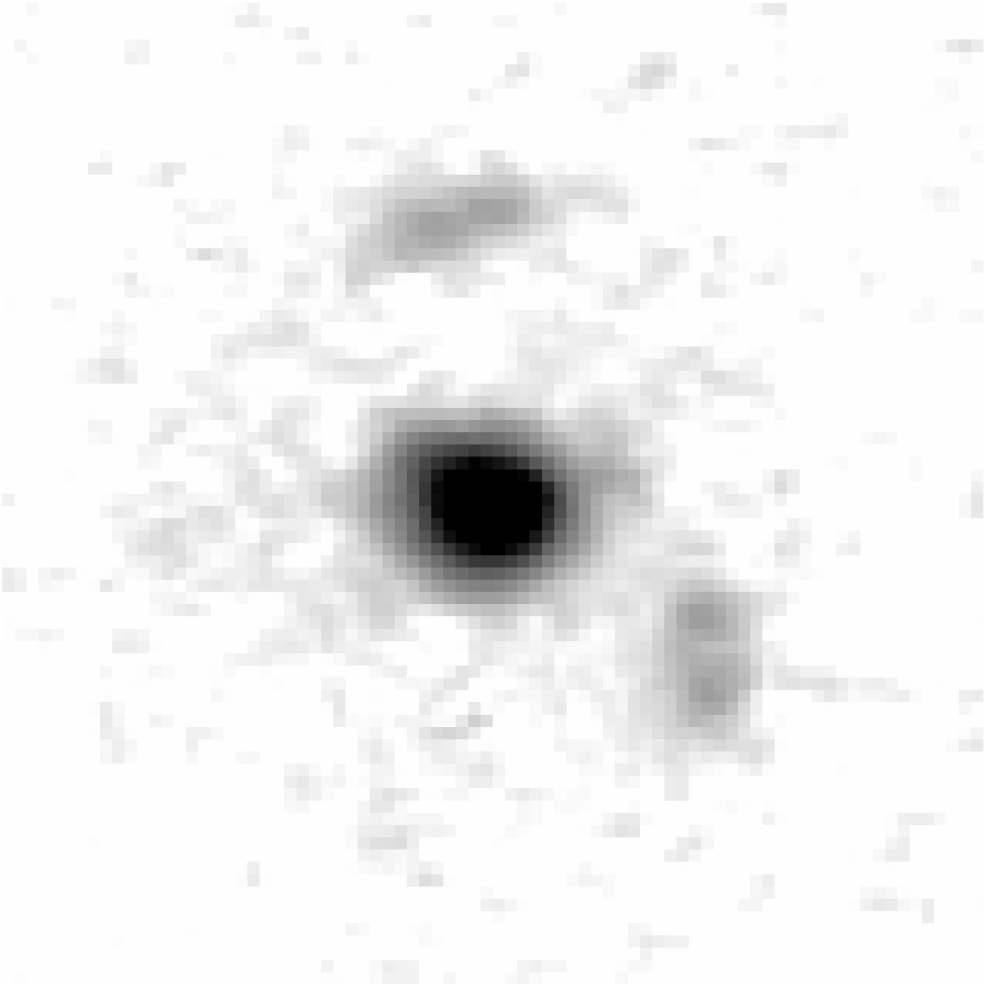

Figure 3.17: TKRS 3660 b-band De-projection

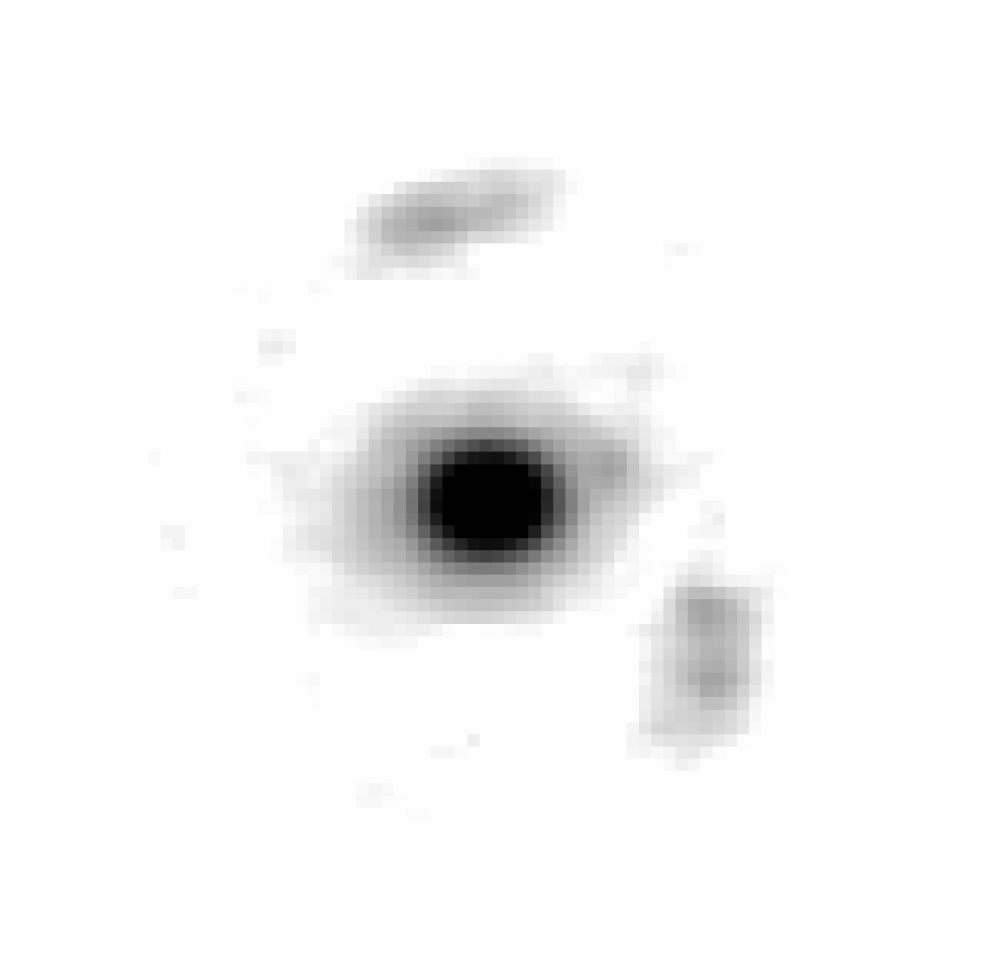

Figure 3.18: TKRS 3660 v-band De-projection

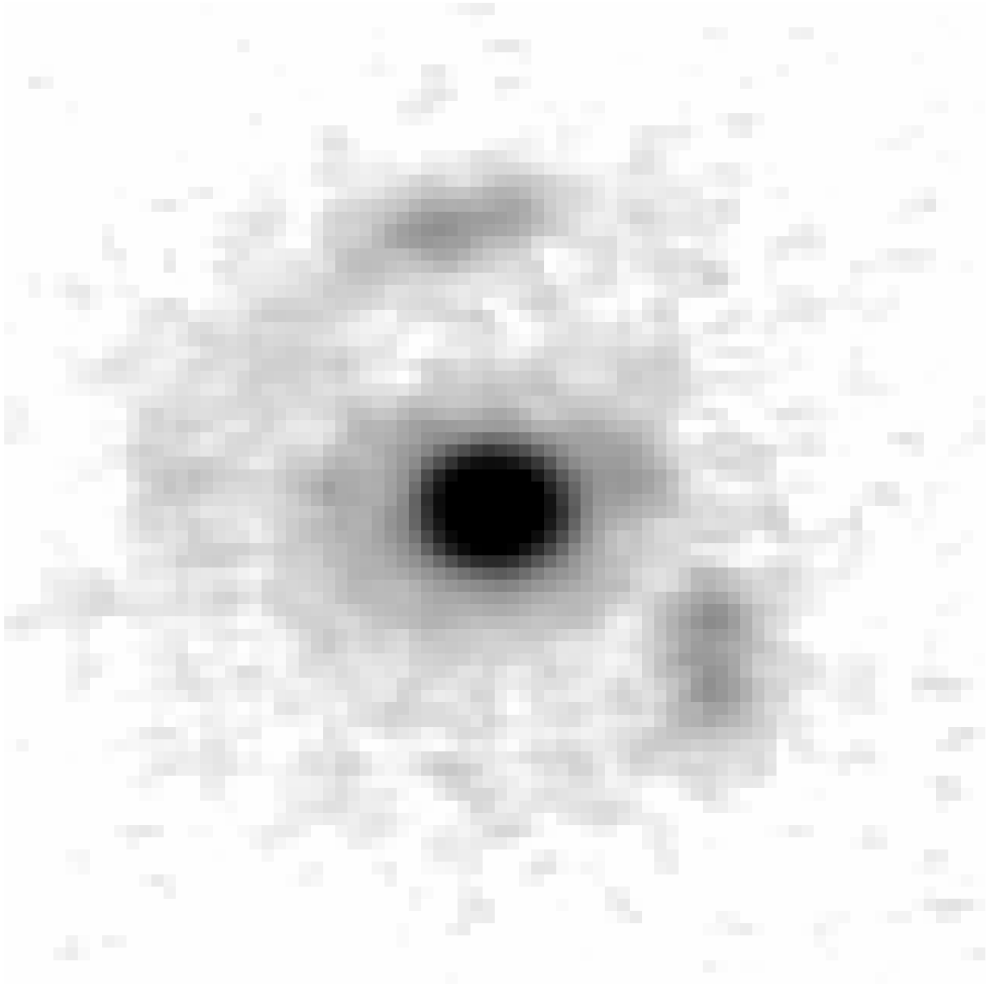

Figure 3.19: TKRS 3660 i-band De-projection

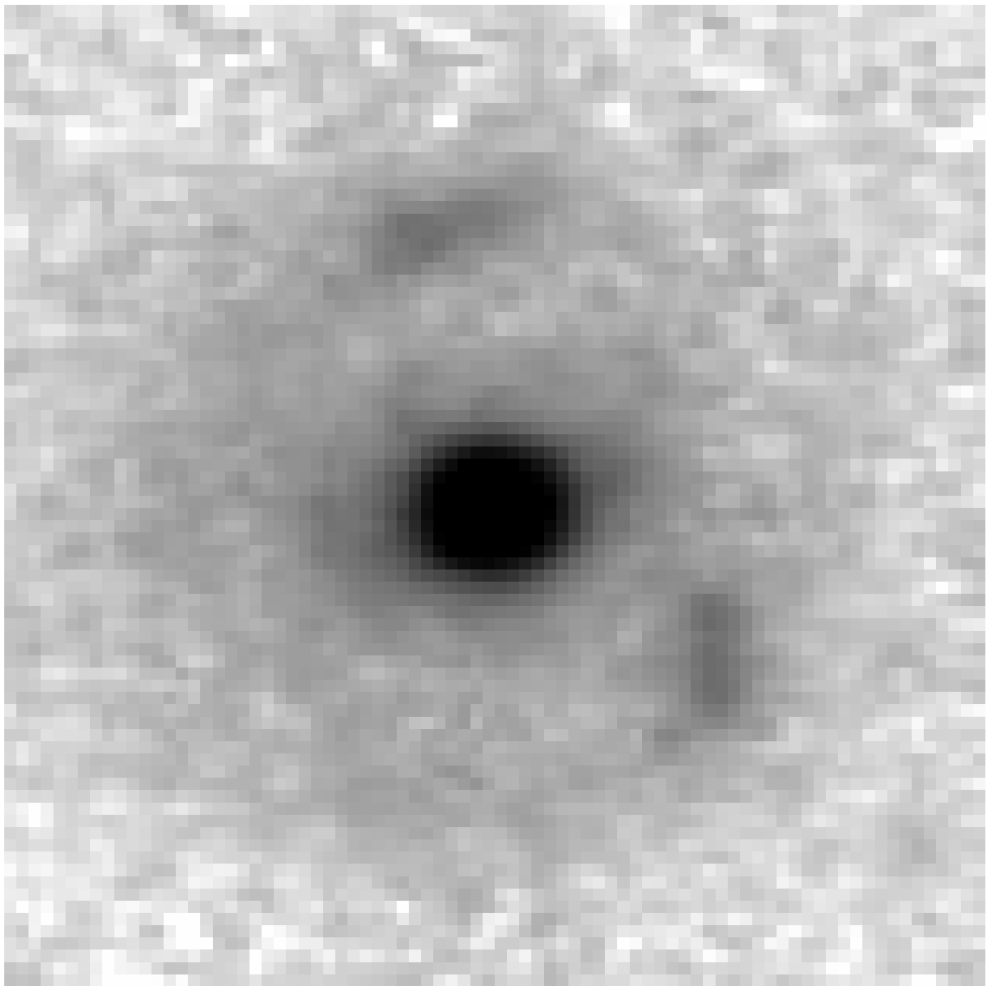

Figure 3.20: TKRS 3660 z-band De-projection

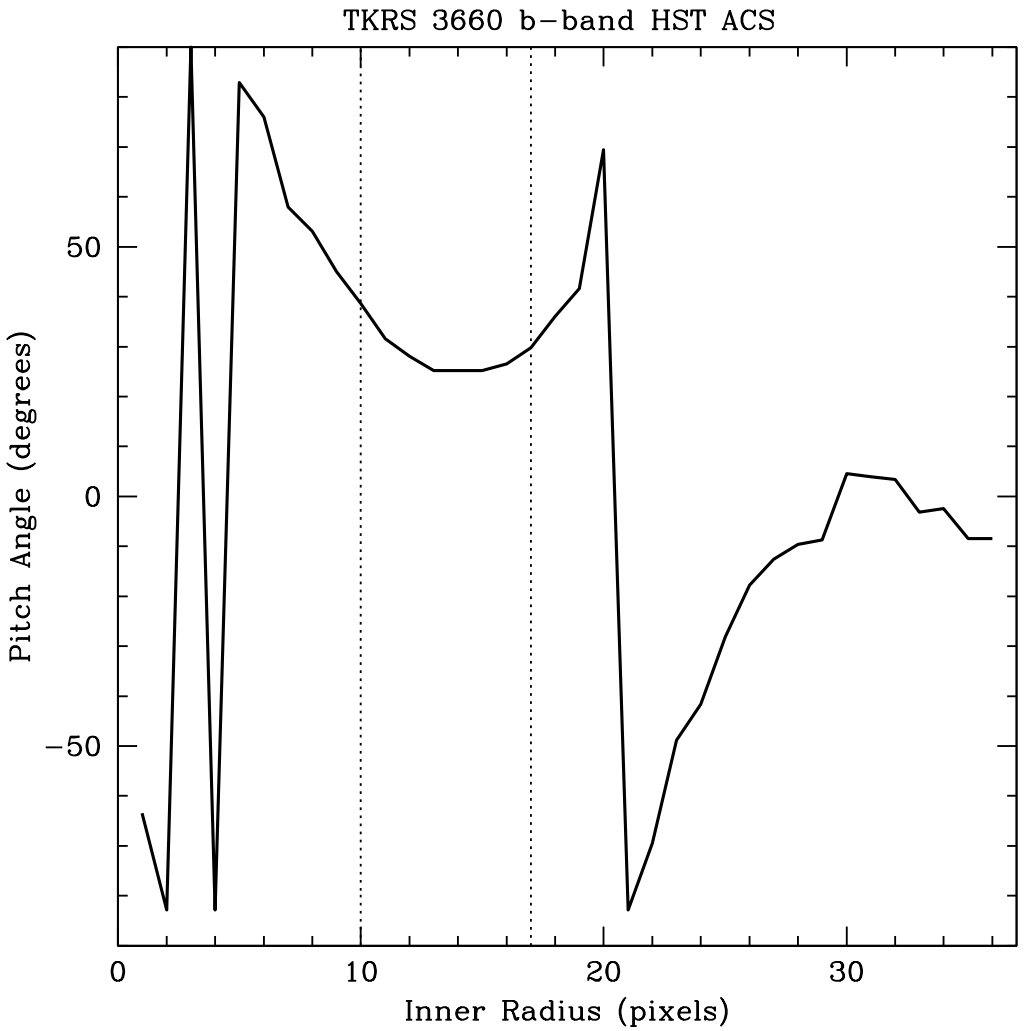

Figure 3.21: Inner Radius vs. Pitch Angle TKRS 3660 b-band

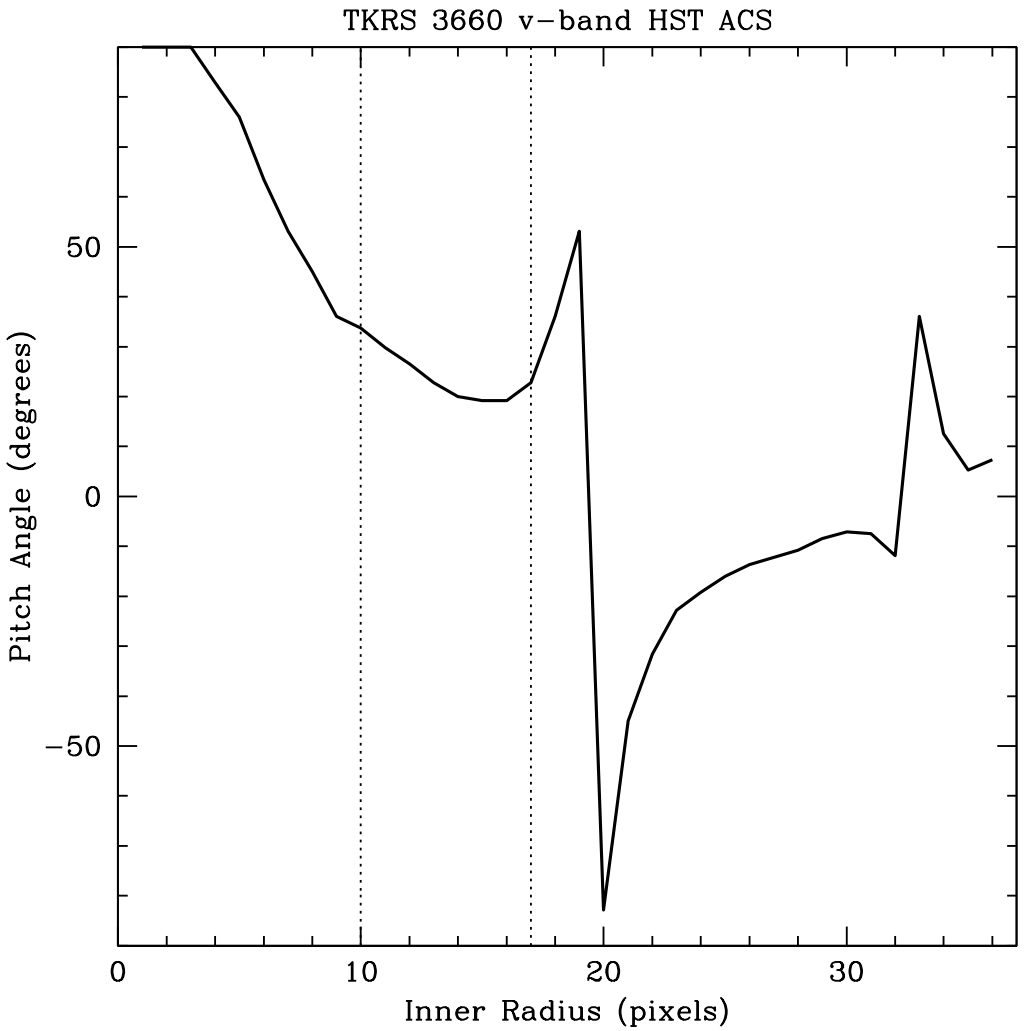

Figure 3.22: Inner Radius vs. Pitch Angle TKRS 3660 v-band

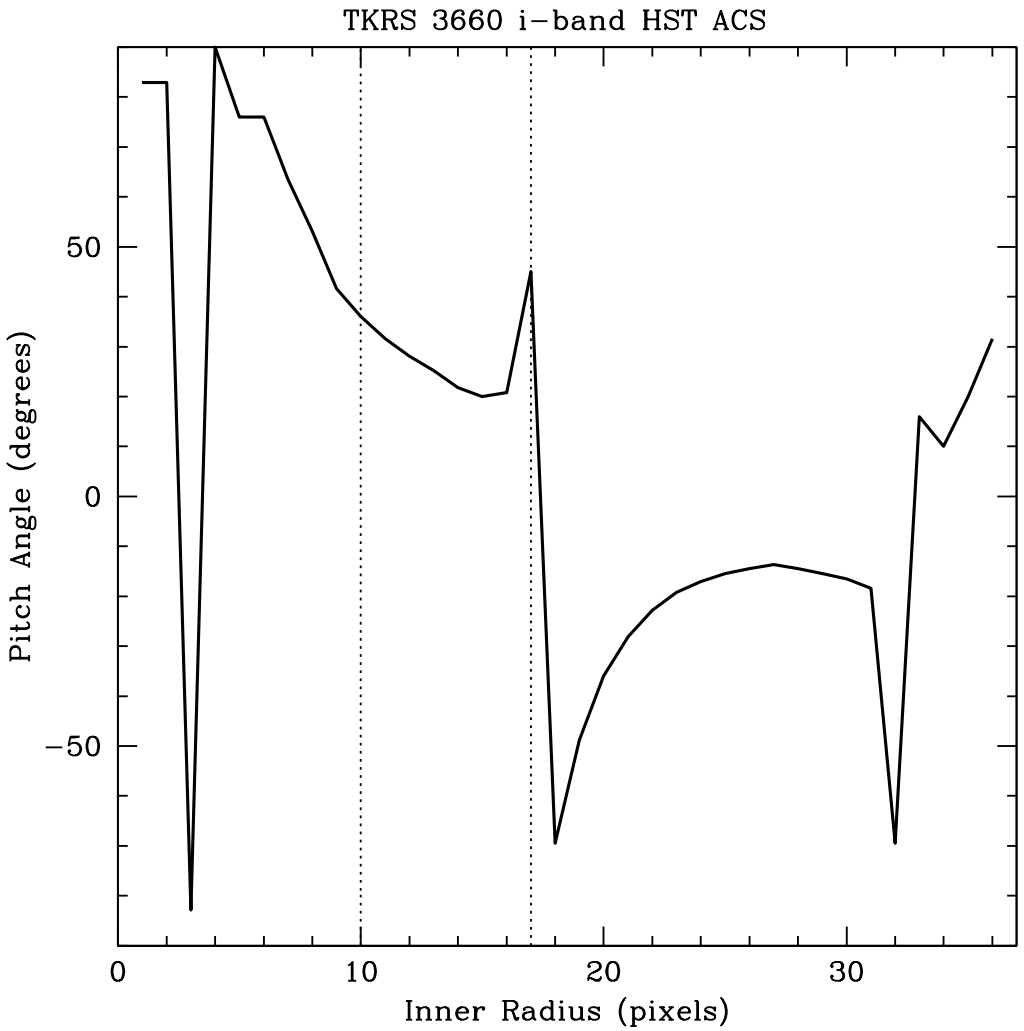

Figure 3.23: Inner Radius vs. Pitch Angle TKRS 3660 i-band

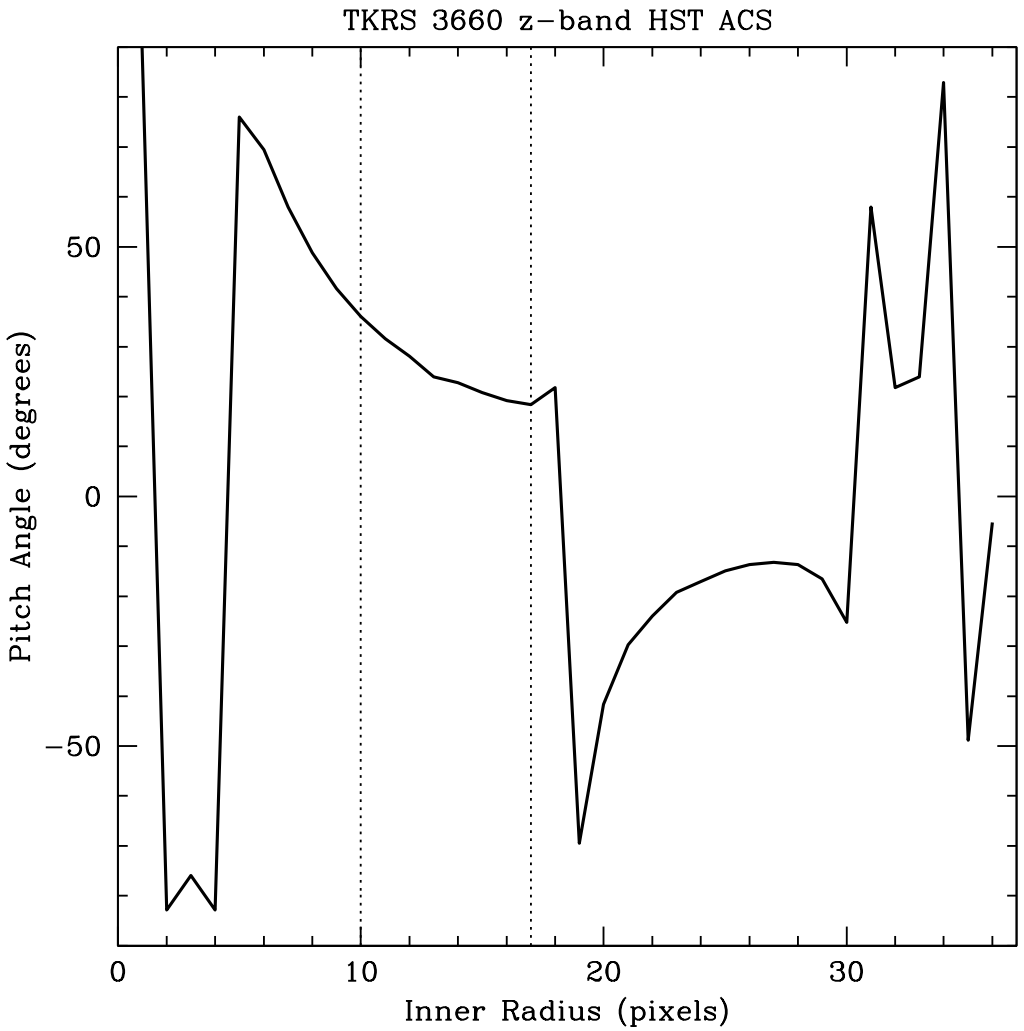

Figure 3.24: Inner Radius vs. Pitch Angle TKRS 3660 z-band

3.2 Estimating Mass

With a mass scaling relationship, the black hole mass can be estimated from a single spectrum giving the ability to make a large sample size of black hole masses for evolution studies.

We will explain the techniques for calculating the central mass of the AGN. These techniques are mass scaling relationships derived from reverberation mapping. In order to determine the mass of black holes at greater distances, a relationship was established between the width of broad lines in the emission spectra and the velocity of material orbiting the accretion disk. Another relationship established was the continuum luminosity of the central region and the distance at which this material is orbiting the central massive object.

These mass scaling relationships are formed from reverberation mapping used to measure the radius of the broad emission-line orbiting region by measuring the time delay between continuum and emission line variations (Peterson, 2001). Doppler measures of the velocity of material in a Keplerian orbit around the central mass are then used, as well, to estimate the mass of the central concentration (Peterson, 2001). A continuum luminosity is measured at 5100Å or 3100Å, depending on the scaling relation being used. Broad line region luminosity relations have been carried out by Kaspi et al. (2005) with reverberation mapping, with which the relation holds.

The broadening of the MgII spectral line is theorized to be broadened by gas surrounding the accretion disk of the central supermassive black hole (SMBH). This gas is orbiting around in the broad line region of the AGN according to the AGN standard model. The lack of forbidden emission lines in the broad line region tells us the density is greater in this region compared to regions with forbidden lines.

McLure & Jarvis (2002) publish the following mass scaling relationship formula

$$\frac{M_{bh}}{M_{\odot}} = 3.37(\frac{\lambda L_{3000}}{10^{37}W})^{0.47}[\frac{FWHMMgII}{kms^{-1}}]^2 \tag{3.1}$$

and McGill et al. (2008) published the mass scaling relationship which was used by Bennert et al. (2011):

$$\log M_{BH} = 6.767 + 2\log(\frac{FWHM_{MgII}}{1000kms^{-1}}) + 0.47\log\frac{\lambda L_{3000}}{10^{44}ergs^{-1}}. \tag{3.2}$$

We calculate the AGN luminosity from the continuum flux at 3000Å and the distance

luminosity, (D_L), calculated with the given cosmology, where as Bennert et al. (2011) derives it from the PSF magnitude based on the AGN SED from Berk et al. (2001). The FWHM is measured from the Doppler corrected spectra with the Fe emission subtracted using a template fitting technique. Bennert et al. (2011) did not attempt to subtract the Fe emission and instead gave an error by which the FWHM is underestimated based on the nature of the measurement.

3.2.1 Szokoly 15

Szokoly 15 is located in the GOODS-S section 12 with coordinates (6029, 6234) and J2000 coordinates J033252.88-275119.8. Hasan (2007) gives Szokoly 15 a spectroscopic quality factor of "1: secure." Szokoly et al. (2004) provides optical spectroscopy for the AGN which exhibits a broad MgII emission line giving a redshift of 1.227000. The NASA/IPAC Extragalactic Database (NED)[1] does not show spectra available and list the source under its COMBO-17 number 26470. RA and DEC are listed as 03h32m52.9s -27d51m20s and a Vega magnitude and filter as 22.62 and R-band. Véron-Cetty & Véron (2006) classifies the galaxy as a Seyfert I AGN with broad lines. Szokoly et al. (2004) captured spectra twice for the AGN on mask 15 with quality 0.0 and mask 137 with quality 1.0 and gives an optical classification of BLAGN and an X-ray classification of AGN-1. The MgII emission line is difficult to see with the noise nearly greater than the signal, but with the broadening of the emission line it is still detectable. With a box smoothing of 11 the MgII emission line distinguishes itself. We then measure a FWHM of the MgII emission line after the smoothing. The MgII region is also where Fe emission lines are found and without accounting for, we will underestimate the full width at half max because the base of the MgII line is drown out by the Fe emission.

Bennert et al. (2011) reports a mass of 1.02×10^9 $M_\odot$ with an uncertainty of 0.5 dex. For these masses the AGN luminosity is not measured from the spectra but is derived from a PSF magnitude and then extrapolated based on the assumed AGN composite SED of(Berk et al., 2001; Bennert et al., 2011).

3.2.2 Szokoly 44a

Szokoly 44a is located in GOODS-S, section 35, at (1314, 3138) which corresponds to J2000 coordinates J033226.49-274035.5. The spectra was measured by Szokoly et al. (2004)

[1] ned.ipac.caltech.edu

and shows a redshift at z= 1.031. The non Doppler corrected spectra displays a distinct MgII emission line at 5690Å and is listed by Szokoly et al. (2004) as having a quality flag of 2.0+ which indicates a "reliable redshift determination." The optical classification is listed as BLAGN and the X-ray classification is QSO-1 (Szokoly et al., 2004). The R-band magnitude is quoted as 19.79 and the X-ray luminosity is listed as $44.2log$ erg s^{-1}. The FWHM and flux are measured here in the same way as before but without smoothing or binning.

Bennert et al. (2011) reports a mass of $1.00 \times 10^8 M_\odot$ with an uncertainty of 0.5 dex.

3.2.3 TKRS 3660

TKRS 3660 $12^h35^m53^s$, $+62°10^m37^s$ exhibits MgII emission line broadening. The spiral AGN from GOODS-N had a relatively flux calibrated spectrum ranging from 4704Å to 9884Å (Cowie et al., 2004). Wirth et al. (2004) list the object as a galaxy with an R-band magnitude of 44.4 and an X-ray luminosity of log 21.79 erg s^{-1} and a redshift of 1.371.

We used two different calibration methods, first with the i-band transmission filter, then the r-band transmission filter from SDSS[2]. The calibration process was completed by passing the standard star BD174708 spectra through the transmission set to get a total flux through the system. This total was then used to calculate the total flux to be seen through the transmission set by applying the magnitude to flux scaling equation. This total flux is then combined as a ratio with the unitless total acquired by passing the relative flux calibrated spectra of TKRS 3660 through the system. We form a scaling relation from the flux total by the relative flux total and then use this value. Then we shift the unitless relative flux calibrated spectra to a unit dependent flux calibrated spectra.

The spectrograph shows a broad MgII emission line with two absorption lines in the center, presumably the two line components, at 2795.528Å and 2802.705Å. We remove these two absorption lines before measuring the FWHM and measure the flux in the same way as before.

After fitting and subtracting an Fe template from the spectra we measure a Gaussian FWHM at 2810Å of 5658 km s^{-1}.

Bennert et al. (2011) reports a mass of 2.57 $\times$ 10^8 $M_{\backslash}odot$ with an uncertainty of 0.5 dex.

[2]http://classic.sdss.org/dr7/instruments/imager

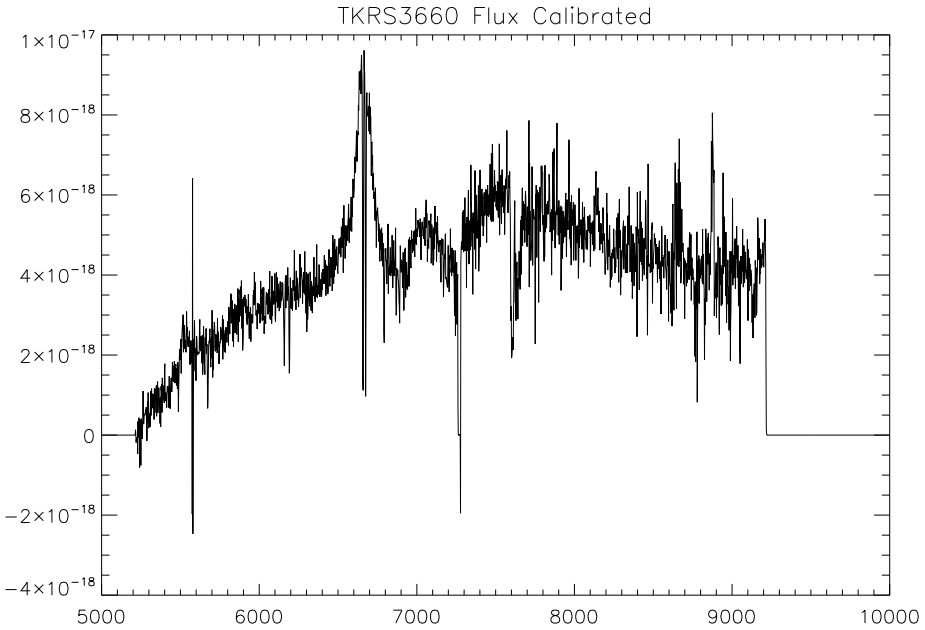

Figure 3.25: TKRS 3660 Flux Calibrated Spectra

3.3 Results

The Seigar et al. (2008); Berrier et al. (2013) relationship between a spiral galaxies P and central M_{BH} relationship holds for the local galaxies, $z \approx 0$. Here we attempt to determine if the relationship holds for galaxies at $z \approx 1$ by measuring the pitch angle for the selected distant galaxies.

$$\log_{10} M_{bh} = (8.44 \pm 0.10) - (0.076 \pm 0.005)P \tag{3.3}$$

(Seigar et al., 2008)

Three distant spiral active galaxies have been analyzed in order to quantitatively describe the tightness of the spiral structure. The $M - P$ relationship from Berrier et al. (2013) is then used to show the spiral arm pitch angle is related to the black hole mass estimate from McLure & Jarvis (2002) mass scaling relationship.

As these three distant galaxies are shown to fit the $M - P$ relationship of nearby galaxies, further data points of distant galaxies may extend the relationship and therefore be a useful tool in studying the evolution of supermassive black holes in spiral galaxies with a single image of the spiral structure. In this way, a census of supermassive black holes could be measured as a function of look-back time with existing images or limited telescope time

MgII BLAGN Spiral Structure

Objects	z	D_L	FWHM$_{MgII}$	$\lambda\ L_{3000}$	M$_{BH}$	FWHM$_{MgII}$	$\lambda\ L_{3000}$	M$_{BH}$
(1)	(2)	(3)	(4)	(5)	(6)	(7)	(8)	(9)
		Mpc	(km s^{-1})	(10^{44} erg s^{-1})	(log $\frac{M_{BH}}{M_\odot}$)	(km s^{-1})	(10^{44} erg s^{-1})	(log $\frac{M_{BH}}{M_\odot}$)
SHBH 00015	1.227	8516	16208	0.43	9.01	11862	0.0104	7.74
SHBH 00044a	1.031	6892	2430	9.51	8.00	2371	0.00136	5.93
TKRS 03660	1.371	9900	5441	2.32	8.41	5658	0.140	7.63

Table 3.1: Column 1: Object ID from NEDS; [SBH] Szokoly, Bergeron, Hasinger; [TKRS] Team Keck Redshift Survey. Column 2: Spectroscopic Redshift. Column 3: Luminosity Distance. Column 4 & 5 & 6: Bennert et al. (2011). Column 4 & 7: Full Width at Half Maximum of Mg$_{II}$. Column 8: Luminosity at 3000 Angstroms. Column 9 : McLure & Jarvis (2002) Mass Scaling Relation with Error $\pm$ 0.5 dex.

Broad Line Active Galactic Nuclei with Spiral Structure			
GOODS ID	z	$P \pm error$	Comments
J033252.89-275119.9	1.227	-10.3 ± 1.0	Szokoly 15
J033226.49-274035.6	1.031	$+37.7 \pm 7.1$	Szokoly 44a
J123553.12+621037.5	1.371	$+26.7 \pm 6.2$	TKRS 3660

Table 3.2: Column 1: GOODS Object Name. Column 2: Spectroscopic Redshift. Column 3: Spiral Arm Pitch Angle with Error. Column 4: Spectroscopic Survey Object Name

with the equation

$$\log \frac{M}{M_{\odot}} = (8.21 \pm 0.16) - (0.062 \pm 0.009)P \tag{3.4}$$

Berrier et al. (2013).

The measurements here have been calculated using a cosmology of a flat universe, $\omega_m h^2 = 0.1347$, $\omega_\lambda = 0.728$, $\omega_b = 0.0455$, and $H_0 = 70.4$ kms$^{-1}Mpc^{-1}$.

Presented here are data points to be added to the Berrier et al. (2013) sample which are at greater distances in order to test the relationships robustness at greater look-back times. Although the mass scaling relationship is not a direct measure of the black hole, it is the most reliable estimate of supermassive black hole mass at these distances, next to reverberation mapping, which is a telescope time consuming process. Through reverberation mapping efforts, a scaling relationship has been formed between the continuum luminosity and the orbital radius of the broad line region (Vestergaard, 2002; McLure & Jarvis, 2002) .

Because the mass scaling relationships are based on reverberation mapping, I will first discuss the uncertainties in this method. Uncertainties arising in the reverberation mapping technique from variables such as luminosity distance, time delay between continuum fluctuation and ionization flux fluctuation, and the subtraction of host galaxy star light from the AGN central source luminosity. The unified model of AGN also provides uncertainties from the foundations of all we observe, assuming that all AGN are similar. First of all, errors arise from the fact that the mass scaling relationship is using a relationship of its own. The relationship between the reverberation mapped time delay and the radius at which the broad line region gas orbits the black hole accretion area is a small contribution to the error compared to the luminosity distance for the intermediate to high redshift objects. The mass scaling relationship uses the broad line FWHM as a proxy for the orbital velocity of the

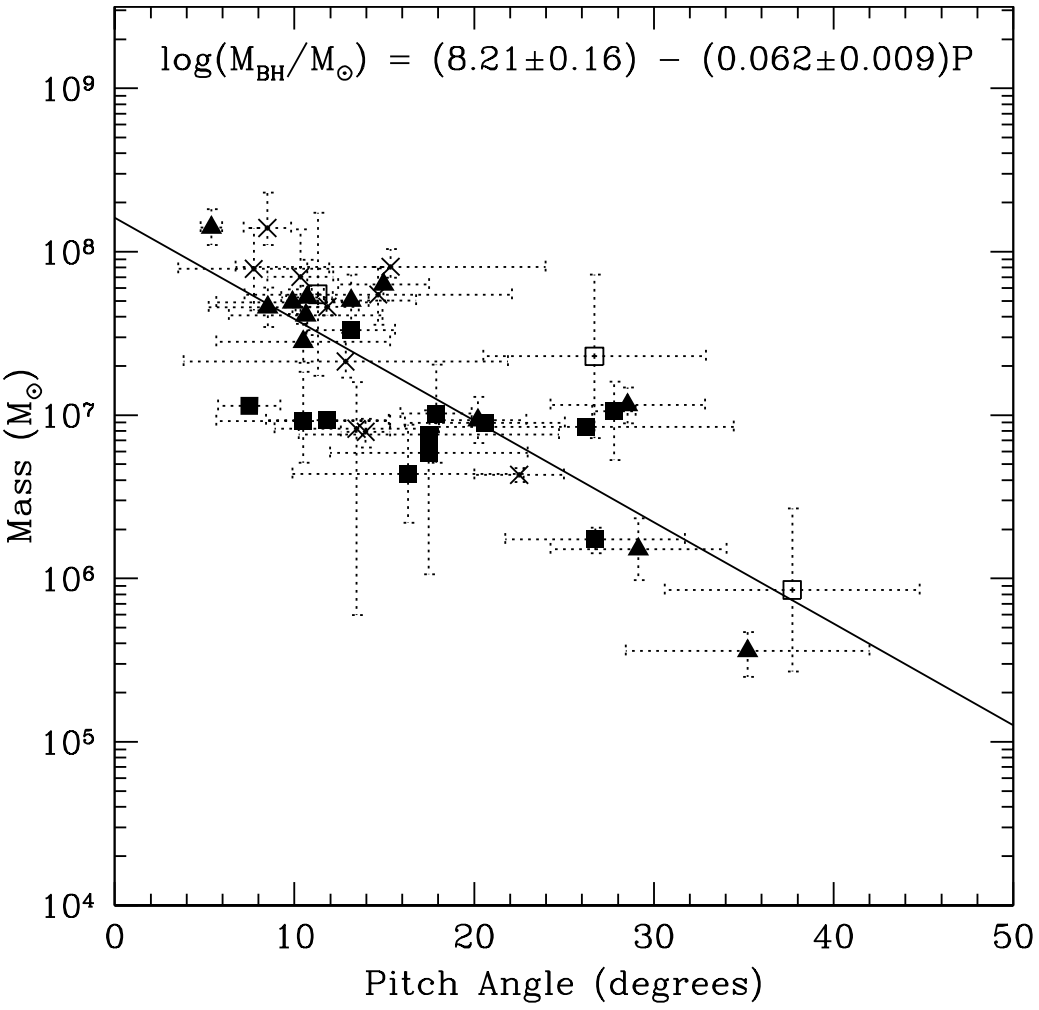

Figure 3.26: The solid squares, triangles and x-marks are from Berrier et al. (2013) and the hollow squares are the three BLAGN from this study.

broad line region and the continuum luminosity at a selected wavelength as a proxy for the broad line region orbital radius. The continuum luminosity is measured and dependent on the accuracy of the luminosity distance measurement, providing a substantial portion of the error for mass scaling relationship black hole mass estimates.

4 Conclusion

A significant sample of black hole masses through the age of the universe would help in understanding how these objects grew throughout the life time of the universe with the knowledge of the black hole growth corresponding to the growth of the galaxy as a whole. This information would also enlighten our understanding of the entire galaxies evolution throughout the age of the universe. So with the $M - P$ relationship, a black hole mass function can be created for spiral galaxies where spiral arms are visible, which would greatly increase the sample size of black hole masses at high redshift. With this information, we hope to better understand previous observations of black hole masses which tend to be less massive the farther back in time we look, cosmic downsizing. Most mass measurements have been carried out on high luminosity galaxies, which would create a bias toward the more massive black holes, i.e. a selection effect. The $M - P$ relation could help to fill the gap between active galaxies and quiescent galaxies.

Another question to be investigated is whether or not the clustering of galaxies and the dark matter halo interactions within a densely populated area affects the morphology of the galaxies. This may be investigated by quantifying the spiral arm pitch angle of spiral galaxies within the cluster and studying it as a function of dark matter halo mass, cluster size or distance.

Bibliography

Alexander, D. M., Bauer, F. E., Brandt, W. N., Schneider, D. P., Hornschemeier, A. E., Vignali, C., Barger, A. J., Broos, P. S., Cowie, L. L., Garmire, G. P., Townsley, L. K., Bautz, M. W., Chartas, G., & Sargent, W. L. W. 2003, The Astronomical Journal, 126, 539

Barger, A. J., Cowie, L. L., & Wang, W.-H. 2008, The Astrophysical Journal, 689, 687

Bennert, V. N., Auger, M. W., Treu, T., Woo, J.-H., & Malkan, M. A. 2011, The Astrophysical Journal, 726, 59

Bentz, M. C., Peterson, B. M., Pogge, R. W., Vestergaard, M., & Onken, C. A. 2006, The Astrophysical Journal, 644, 133

Berk, D. E. V., Richards, G. T., Bauer, A., Strauss, M. A., Schneider, D. P., Heckman, T. M., York, D. G., Hall, P. B., Fan, X., Knapp, G. R., Anderson, S. F., Annis, J., Bahcall, N. A., Bernardi, M., Briggs, J. W., Brinkmann, J., Brunner, R., Burles, S., Carey, L., Castander, F. J., Connolly, A. J., Crocker, J. H., Csabai, I., Doi, M., Finkbeiner, D., Friedman, S., Frieman, J. A., Fukugita, M., Gunn, J. E., Hennessy, G. S., Ivezić, Ž., Kent, S., Kunszt, P. Z., Lamb, D. Q., Leger, R. F., Long, D. C., Loveday, J., Lupton, R. H., Meiksin, A., Merelli, A., Munn, J. A., Newberg, H. J., Newcomb, M., Nichol, R. C., Owen, R., Pier, J. R., Pope, A., Rockosi, C. M., Schlegel, D. J., Siegmund, W. A., Smee, S., Snir, Y., Stoughton, C., Stubbs, C., SubbaRao, M., Szalay, A. S., Szokoly, G. P., Tremonti, C., Uomoto, A., Waddell, P., Yanny, B., & Zheng, W. 2001, The Astronomical Journal, 122, 549

Berrier, J. C., Davis, B. L., Kennefick, D., Kennefick, J. D., Seigar, M. S., Barrows, R. S., Hartley, M., Shields, D., Bentz, M. C., & Lacy, C. H. S. 2013, The Astrophysical Journal, 769, 132

Bianchi, S., Maiolino, R., & Risaliti, G. 2012, Advances in Astronomy, 2012, 17

Burbidge, G. R., Burbidge, E. M., & Sandage, A. R. 1963, Reviews of Modern Physics, 35, 947

Carroll, B. W. & Ostlie, D. A. 2007, An Introduction to Modern Astrophysics (Addison Wesley Pearson)

Cowie, L. L., Barger, A. J., Hu, E. M., Capak, P., & Songaila, A. 2004, The Astronomical Journal, 127, 3137

Davis, B. L., Berrier, J. C., Shields, D. W., Kennefick, J., Kennefick, D., Seigar, M. S., Lacy, C. H. S., & Puerari, I. 2012, The Astrophysical Journal Supplement, 199, 33

Elvis, M., Wilkes, B. J., McDowell, J. C., Green, R. F., Bechtold, J., Willner, S. P., Oey, M. S., Polomski, E., & Cutri, R. 1994, The Astrophysical Journal Supplement Series, 95, 1

Ferrarese, L. & Merritt, D. 2000, The Astrophysical Journal, 539, L9

Garmire, G. P., Bautz, M. W., Ford, P. G., Nousek, J. A., & Ricker, G. R. 2003, X-Ray and Gamma-Ray Telescopes and Instruments for Astronomy. Edited by Joachim E. Truemper, 4851, 28

Gebhardt, K., Bender, R., Bower, G., Dressler, A., Faber, S. M., Filippenko, A. V., Green, R., Grillmair, C., Ho, L. C., Kormendy, J., Lauer, T. R., Magorrian, J., Pinkney, J., Richstone, D., & Tremaine, S. 2000, The Astrophysical Journal, 539, L13

Ghez, A. M., Salim, S., Hornstein, S. D., Tanner, A., Lu, J. R., Morris, M., Becklin, E. E., & Duchêne, G. 2005, The Astrophysical Journal, 620, 744

Giacconi, R., Rosati, P., Tozzi, P., Nonino, M., Hasinger, G., Norman, C., Bergeron, J., Borgani, S., Gilli, R., Gilmozzi, R., & Zheng, W. 2001, The Astrophysical Journal, 551, 624

Giavalisco, M., Ferguson, H. C., Koekemoer, A. M., Dickinson, M., Alexander, D. M., Bauer, F. E., Bergeron, J., Biagetti, C., Brandt, W. N., Casertano, S., Cesarsky, C., Chatzichristou, E., Conselice, C., Cristiani, S., Costa, L. D., Dahlen, T., de Mello, D., Eisenhardt, P., Erben, T., Fall, S. M., Fassnacht, C., Fosbury, R., Fruchter, A., Gardner, J. P., Grogin, N., Hook, R. N., Hornschemeier, A. E., Idzi, R., Jogee, S., Kretchmer, C., Laidler, V., Lee, K. S., Livio, M., Lucas, R., Madau, P., Mobasher, B., Moustakas, L. A., Nonino, M., Padovani, P., Papovich, C., Park, Y., Ravindranath, S., Renzini, A., Richardson, M., Riess, A., Rosati, P., Schirmer, M., Schreier, E., Somerville, R. S., Spinrad, H., Stern, D., Stiavelli, M., Strolger, L., Urry, C. M., Vandame, B., Williams, R., & Wolf, C. 2004, The Astrophysical Journal, 600, L93

Greenstein, J. L. & Schmidt, M. 1964, Astrophysical Journal, 140, 1

Hasan, P. 2007, Astrophysics and Space Science, 312, 63

Hazard, C. 1964, Nature, 202, 227

Hubble, E. 1929, Proceedings of the National Academy of Sciences of the United States of America, 15, 168

Kaspi, S., Maoz, D., Netzer, H., Peterson, B. M., Vestergaard, M., & Jannuzi, B. T. 2005, The Astrophysical Journal, 629, 61

Kormendy, J., Gebhardt, K., & Richstone, D. 2000, American Astronomical Society, 196, 702

Kormendy, J. & Richstone, D. 1995, Annual Review of Astronomy and Astrophysics, 33, 581

Krolik, J. H. & Begelman, M. C. 1988, Astrophysical Journal, 329, 702

Magorrian, J., Tremaine, S., Richstone, D., Bender, R., Bower, G., Dressler, A., Faber, S. M., Gebhardt, K., Green, R., Grillmair, C., Kormendy, J., & Lauer, T. 1998, The Astronomical Journal, 115, 2285

McGill, K. L., Woo, J.-H., Treu, T., & Malkan, M. A. 2008, The Astrophysical Journal, 673, 703

McLure, R. J. & Jarvis, M. J. 2002, Monthly Notice of the Royal Astronomical Society, 337, 109

Osterbrock, D. E. & Ferland, G. J. 2006, Astrophysics of Gaseous Nebulae and Active Galactic Nuclei, 2nd edn. (University Science Books)

Peterson, B. M. 1993, PASP, 105, 247

—. 1997, An introduction to active galactic nuclei, iSBN: 0521473489

—. 2001, Advanced Lectures on the Starburst-AGN Connection, 3

Peterson, B. M., Ferrarese, L., Gilbert, K. M., Kaspi, S., Malkan, M. A., Maoz, D., Merritt, D., Netzer, H., Onken, C. A., Pogge, R. W., Vestergaard, M., & Wandel, A. 2004, The Astrophysical Journal, 613, 682

Schmidt, M. 1963, Nature, 197, 1040

Seigar, M. S., Kennefick, D., Kennefick, J., & Lacy, C. H. S. 2008, The Astrophysical Journal, 678, L93, (c) 2008: The American Astronomical Society

Seyfert, C. K. 1946, Publications of the American Astronomical Society, 10, 317

Shields, D. W., Hughes, J. A., Barrows, R. S., Berrier, J., Davis, B., Kennefick, D., Kennefick, J., Ring, W., Seigar, M., & Survey, A. G. E. 2010, American Astronomical Society, 215, 381

Szokoly, G. P., Bergeron, J., Hasinger, G., Lehmann, I., Kewley, L., Mainieri, V., Nonino, M., Rosati, P., Giacconi, R., Gilli, R., Gilmozzi, R., Norman, C., Romaniello, M., Schreier, E., Tozzi, P., Wang, J. X., Zheng, W., & Zirm, A. 2004, The Astrophysical Journal Supplement Series, 155, 271

Tadhunter, C. 2008, New Astronomy Reviews, 52, 227

Treister, E., Urry, C. M., Chatzichristou, E., Bauer, F., Alexander, D. M., Koekemoer, A., Duyne, J. V., Brandt, W. N., Bergeron, J., Stern, D., Moustakas, L. A., Chary, R.-R., Conselice, C., Cristiani, S., & Grogin, N. 2004, The Astrophysical Journal, 616, 123

Trump, J. R., Impey, C. D., Kelly, B. C., Civano, F., Gabor, J. M., Diamond-Stanic, A. M., Merloni, A., Urry, C. M., Hao, H., Jahnke, K., Nagao, T., Taniguchi, Y., Koekemoer, A. M., Lanzuisi, G., Liu, C., Mainieri, V., Salvato, M., & Scoville, N. Z. 2011, Astrophysical Journal, 733, 60

Urry, C. M. & Padovani, P. 1995, Publications of the Astronomical Society of the Pacific, 107, 803

Véron-Cetty, M.-P. & Véron, P. 2006, Astronomy and Astrophysics, 455, 773

Vestergaard, M. 2002, The Astrophysical Journal, 571, 733

Vestergaard, M. & Peterson, B. M. 2006, The Astrophysical Journal, 641, 689

Weisskopf, M. C., Tananbaum, H. D., Speybroeck, L. P. V., & O'Dell, S. L. 2000, Proc. SPIE Vol. 4012, 4012, 2

Wilkes, B. J., Schmidt, G. D., Smith, P. S., Mathur, S., & McLeod, K. K. 1995, Astrophysical Journal Letters v.455, 455, L13

Wirth, G. D., Willmer, C. N. A., Amico, P., Chaffee, F. H., Goodrich, R. W., Kwok, S., Lyke, J. E., Mader, J. A., Tran, H. D., Barger, A. J., Cowie, L. L., Capak, P., Coil, A. L., Cooper, M. C., Conrad, A., Davis, M., Faber, S. M., Hu, E. M., Koo, D. C., Mignant, D. L., Newman, J. A., & Songaila, A. 2004, arXiv, astro-ph

A Description of Research for Popular Publication

Although our understanding of the universe may seem complete, there are many questions yet unsolved. One of these questions pertains to our understanding of the growth of galaxies. In astrophysics the ability to look at galaxies as they were billions of years ago gives them a window into the past. With that being said, the difficulty arises in seeing the galaxies, like our own, at these great distances or look-back times. Because all of the galaxies in our neighborhood of the universe are relatively dim compared to quasars and AGN, it is very difficult and sometimes impossible to detect the dim galaxies at great distances. In this study, we are able to use these very bright galaxies to expand our understanding of their early growth back to about 6 billion years. We find that some of the characteristics observed in nearby galaxies also hold true for these distant galaxies such as the relationship between the tightness of a spiral galaxies arm and the mass of the central supermassive black hole. As we continue to find more galaxies to study and develop larger telescopes we will unlock some of the unsolved mysteries about our universe.

B All Publications Published, Submitted, and Planned

Shields et al. (2010)